LBL-17899 c.2

Lawrence Berkeley Laboratory

UNIVERSITY OF CALIFORNIA

Physics Division

RECEIVED
LAWRENCE
BERKELEY LABORATORY

JUL 23 1984

LIBRARY AND
DOCUMENTS SECTION

Invited talk presented at the Europhysics Topical Conference on Flavor Mixing in Weak Interactions, Palermo, (Erice), Italy, March 4-11, 1984

NEW RESULTS ON FLAVOR PRODUCTION AT PEP

A. Barbaro-Galtieri

May 1984

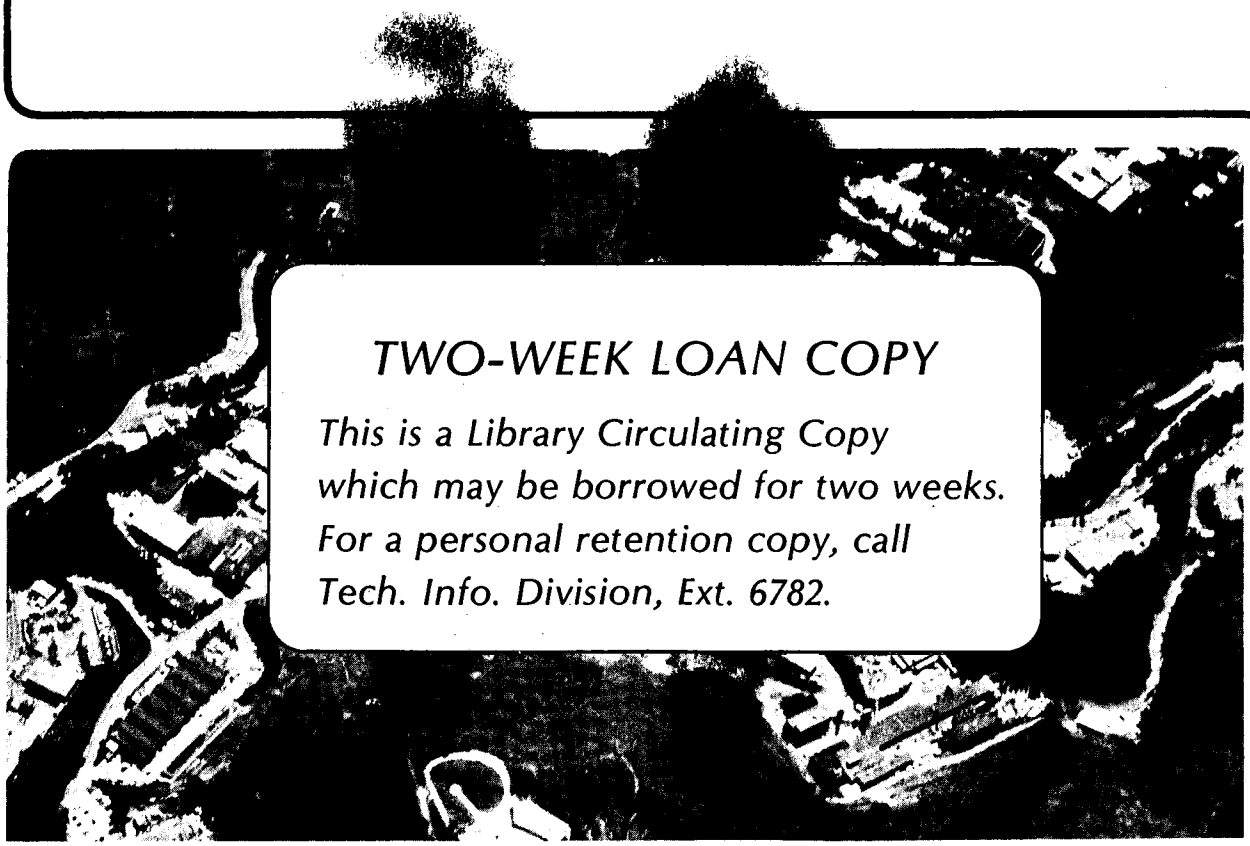

TWO-WEEK LOAN COPY

This is a Library Circulating Copy which may be borrowed for two weeks. For a personal retention copy, call Tech. Info. Division, Ext. 6782.

LBL-17899 c.2

Prepared for the U.S. Department of Energy under Contract DE-AC03-76SF00098

DISCLAIMER

This document was prepared as an account of work sponsored by the United States Government. While this document is believed to contain correct information, neither the United States Government nor any agency thereof, nor the Regents of the University of California, nor any of their employees, makes any warranty, express or implied, or assumes any legal responsibility for the accuracy, completeness, or usefulness of any information, apparatus, product, or process disclosed, or represents that its use would not infringe privately owned rights. Reference herein to any specific commercial product, process, or service by its trade name, trademark, manufacturer, or otherwise, does not necessarily constitute or imply its endorsement, recommendation, or favoring by the United States Government or any agency thereof, or the Regents of the University of California. The views and opinions of authors expressed herein do not necessarily state or reflect those of the United States Government or any agency thereof or the Regents of the University of California.

1. INTRODUCTION

This report includes results from five PEP detectors: DELCO, HRS, MAC, MARK II and TPC. All, except the TPC, are presently taking data at PEP. The TPC is being upgraded: a new superconducting coil is being installed and other improvements are being implemented.

The results discussed here are either new or improved since the Cornell Conference. Other results from PEP have been reported at this Conference by George Trilling (MARK II) on τ, D^0, and b lifetimes and a new limit on the tau neutrino mass, and by Bill Ford on the MAC measurement of the b lifetime.

Section 2 will discuss new results on Particle Searches and a limit on neutrino generations. Section 3 includes new data on weak couplings of c and b quarks. In Section 4 various new results on hadron production are reported. Section 5 summarizes the new results. All data were obtained in e^+e^- collisions with total energy $\sqrt{s}$=29 GeV.

2. PARTICLE SEARCHES

2.1 Fractionally Charged Particles (TPC)

The TPC collaboration has already reported new upper limits on a search for Q=±4/3 particles [1]. They now have new results on Q=±1/3, ±2/3 particles [2]. Simultaneous measurements of curvature and ionization loss (dE/dx) for each particle produced in the reaction $e^+e^- \rightarrow$hadrons allows the identification of particles with charges different from unity.

Figure 1 shows the scatter plot of dE/dx versus momentum for tracks with more than 80 ionization samples produced in 12000 hadronic events. The average charged multiplicity is 12.6 tracks per event. The dE/dx resolution is 3.7%. The bands populated by known Q=1 particles are clearly visible in Fig. 1. The search for fractionally charged particles is made in two regions outside these bands, (a) between 4 and 8 KeV/cm energy loss and (b) between 24 and 40 KeV/cm. A few tracks fall in region (b), but they are easily rejected as candidates by simple requirements: i) track must point to the primary vertex (reject

LBL-17899
Invited talk presented at the Europhysics Topical Conference on "Flavor Mixing in Weak Interactions," Palermo, (Erice), Italy, March 4-11, 1984

NEW RESULTS ON FLAVOR PRODUCTION AT PEP

A. Barbaro-Galtieri

Lawrence Berkeley Laboratory
University of California
Berkeley, CA 94720

TABLE OF CONTENTS

1. INTRODUCTION

2. PARTICLE SEARCHES
 2.1 Fractionally Charged Particles
 2.2 Selectron Search and Neutrino Counting

3. WEAK COUPLINGS OF b AND c QUARKS
 3.1 D^* and D as Tag for c Quark
 3.2 Leptons as Tag for c and b Quarks
 3.3 Summary

4. HADRON PRODUCTION
 4.1 Heavy Quark Fragmentation
  A. Charm Fragmentation from D^*
  B. Results from Prompt Leptons
  C. Summary
 4.2 Inclusive Particle Production
  A. Single Particle Production
  B. Resonance Production
  C. Summary
 4.3 Characteristics of Proton Production in Jets
 4.4 Two Particle Correlations
  A. Baryon Correlations
  B. Flavor Correlations

5. SUMMARY OF NEW RESULTS FROM PEP

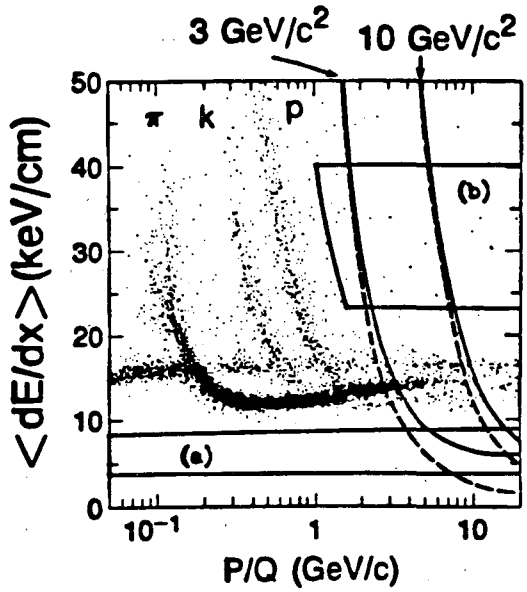

Fig. 1. Ionization loss vs momentum for tracks in jets as measured by the TPC detector [1]. Regions (a) and (b) are search regions for Q=1/3, 2/3 particles. The lines indicate expected <dE/dx> curves for Q=1/3 (dashed) or Q=2/3 (solid) particles with masses of 3 and 10 GeV.

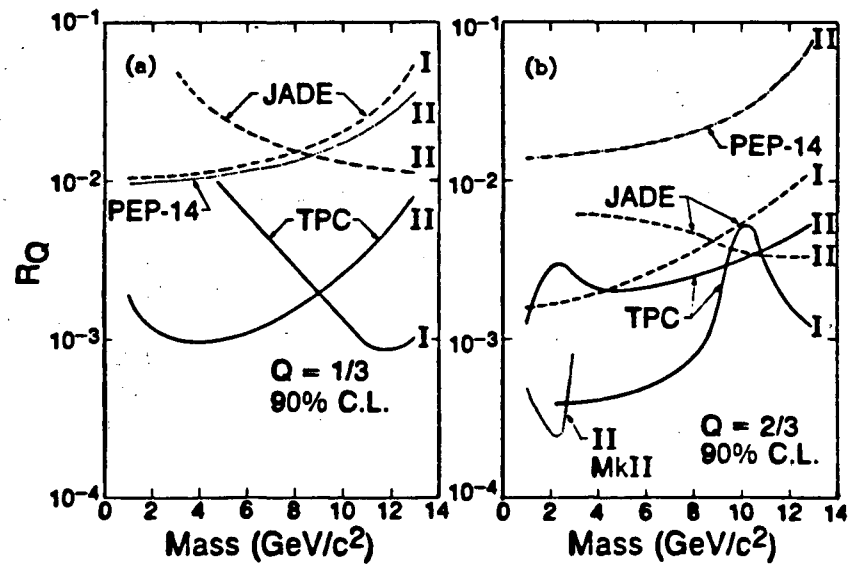

Fig. 2. Upper limits reported by the TPC [2] on production of particles with Q=1/3 (a), and Q=2/3 (b). Results from MARK II, PEP14 and JADE are also shown [3]. Curves labelled I use a momentum distribution $dN/dp \simeq p^2/E$, curves II use $dN/dp \simeq (p^2/E)\exp(-3.5E)$, E in GeV.

deuterons and tritons from secondary interactions), ii) ionization must be due to a single track (reject overlapping tracks). For the total sample of 29000 hadronic events, corresponding to $\int Ldt=77\ pb^{-1}$, no candidates are found.

The upper limits for $|Q|=1/3$, $2/3$ production are shown in Fig. 2 as a function of quark mass. The limits are mass and model dependent since the acceptance of the apparatus is a sharp function of the momentum of the particle. Results for two such models are shown in the figure, as well as limits obtained by other experiments [3] for the reaction $e^+e^- \rightarrow q\bar{q}\ X$.

2.2 Selectron Search and Neutrino Counting (MAC)

The MAC collaboration has new results on their supersymmetric electron search. As previously reported [4] they can extend the selectron mass search to values above the total e^+e^- energy by using the process represented in the diagram of Fig. 3a. The radiative annihilation of e^+e^- into two photinos [5] provides sensitivity, depending on the luminosity, to selectron masses as high as, e.g., 60 GeV at $\sqrt{s}=29$ GeV.

The signature for this reaction is provided by a single gamma in the apparatus and nothing else. The search can only be made above a value of γ energy, E_{min}, where the QED background cannot contribute. The background is due to processes like $e^+e^-\gamma$, $\mu^+\mu^-\gamma$, and $\gamma\gamma\gamma$ where the two leptons or two of the photons escape along the beam pipe. A good acceptance for this process is therefore dependent upon the ability to detect tracks as close as possible to the beam pipe. The variable used is E_T, the transverse energy of the detected photon. The QED background extends to a value of E_T which is related to the smallest veto angle for the photons and leptons of the QED reactions.

The measured E_T spectrum is shown in Fig. 3d. This was obtained with a veto angle $\theta_v \simeq 5^o$, improved from the previous analysis [4] for which $\theta_v = 9^o-12^o$ (Fig. 3c). The integrated luminosity for the new analysis is 34 pb^{-1}. No candidate events are found for $E_T > 3$ GeV. For the old analysis, the minimum γ energy was 3 GeV and the search region was for $E_T >$ 4.3 GeV. The lower limits, for the combined

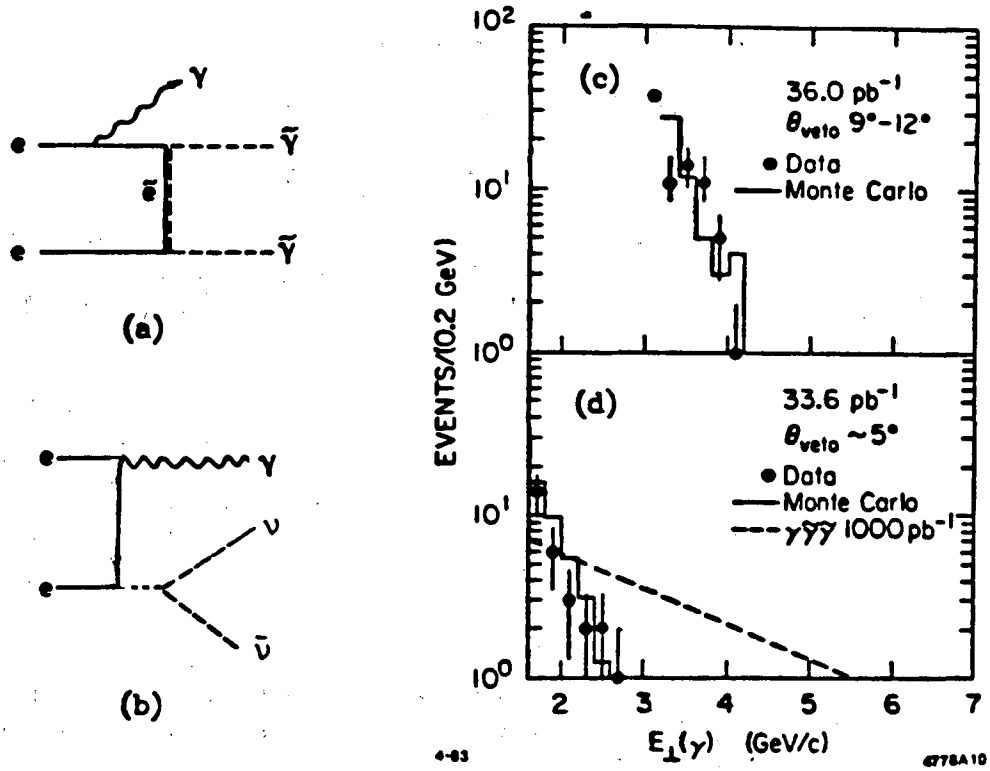

Fig. 3. (a) Radiative (e^+e^-) annihilation into $\tilde{\gamma}\tilde{\gamma}$, used for selectron search, (b) diagram used for neutrino counting, (c) MAC's measured spectrum of transverse energy, for events with one γ only. Solid curve: spectrum of QED background processes. The veto angle was $9^\circ-12^\circ$, (d) same as (c) with veto angle $\cong 5^\circ$. Dashed curve: expected spectrum for $e^+e^- \to \gamma\tilde{\gamma}\tilde{\gamma}$.

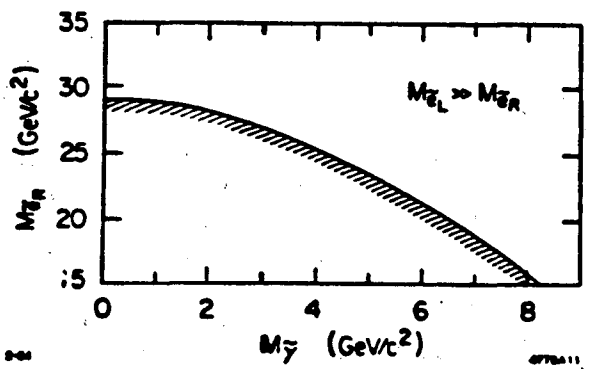

Fig. 4. The region of excluded selectron masses for massive photinos (MAC [4]).

luminosity (73 pb^{-1}) are as follows:

$$m_{\tilde{e}} > 29 \text{ GeV} \quad 90\%\text{CL for } m_L >> m_R,\ m_{\tilde{\gamma}} = 0$$

$$m_{\tilde{e}} > 35 \text{ GeV} \quad 90\%\text{CL for } m_R = m_L,\ m_{\tilde{\gamma}} = 0$$

where m_L and m_R are the masses for the left-handed and right-handed selectron. For heavy photinos, limits lower than these are expected [5]. Figure 4 shows the region of excluded masses for $m_L >> m_R$.

The same data can be used to calculate an upper limit on the number of neutrino generations. The radiative process $e^+e^- \rightarrow \gamma\nu\bar{\nu}$ via a virtual Z^o (Fig. 3b) can be used to estimate the number of light neutrinos [6]. Again, with no candidates found a 90% CL upper limit can be determined:

$$N_\nu < 43$$

For comparison the upper limits set by the UA1 [7] and UA2 [8] experiments in $\bar{p}p$ collisions from the Z^o width measurement are as follows:

UA1	$\Gamma(Z^o) < 8.5$ GeV	$N_\nu < 34$
UA2	$\Gamma(Z^o) < 11$ GeV	$N_\nu < 47$

The UA1 group [7] also estimates the number of neutrino generations from the lower limit of the $Z^o \rightarrow e^+e^-$ branching ratio to be $N_\nu < 18$.

3. WEAK COUPLINGS OF b AND c QUARKS

In e^+e^- annihilation heavy quarks are produced via one photon or Z^o intermediate states. At PEP and PETRA energies the interference between these two production mechanisms is expected to produce a measurable asymmetry in the distribution of the quark production angle with respect to the beam direction.

In lowest order QED, and assuming only one Z^o, the forward-backward asymmetry can be written as follows:

$$(1) \qquad A = (F-B)/(F+B) = -3/2\chi(a_e \cdot a_f)/Q_f$$

where Q_f is the charge of the final quark considered, a_e and a_f are the axial coupling constants for the

electrons and the final quark, and, away from the Z^o pole, χ can be approximated with the expression

$$(2) \qquad \chi = \frac{G_F}{8\pi\alpha\sqrt{2}} \frac{sM^2}{s-M_{Z^o}^2} = -.042 \qquad \text{for } s = \sqrt{29}\ \text{GeV}$$

The standard model predicts $a_e=a_b=-1$, $a_c=+1$.

Two methods have been used to measure this asymmetry: a) use D^* and D^o mesons, products of the c quark, and b) use leptons that are decay products of hadrons produced in the hadronization of c and b quarks.

3.1 D^* and D as Tag for c Quarks (HRS and TPC)

The charm quark is easily tagged by identifying D^* events using the decay

$$(3) \qquad D^{*+} \rightarrow D^o\ \pi^+ \qquad \text{(and c. c.)}$$

with subsequent D^o decay into $K^-\pi^+$, $K^-\pi^+\pi^+\pi^-$, $K^-\pi^+\pi^o$ etc. The decay (3) has a small Q value (5.8 MeV) and the D^*-D mass difference exhibits a narrow peak at the pion mass. The background from u, d, and s quarks will be very small, whereas the contribution from b quark can be calculated to be, depending on the spectrum of D's from bottom quarks, at most

$$b/c = Q_b^{\ 2}/Q_c^{\ 2} = 1/4$$

This method, originally used by the MARK I collaboration [9], has been used extensively in e^+e^- collisions [10-12].

New results from PEP since the Cornell Conference are from TPC [14] and HRS [11]. The TPC results are shown in Fig. 5. Here particle identification is used to identify the kaon, in high momentum $(D^o\pi^+)$ combinations, i.e. $z = 2E_{D^*}/\sqrt{s} > 0.5$. The $D^{*\pm}$ peak includes 120 events, obtained with 77 pb^{-1} of data. The decay modes used are $D^o \rightarrow K^-\pi^+$, $K^-\pi^+\pi^o$ and $K^-\pi^+\pi^+\pi^-$ and the charge conjugate states. For the asymmetry measurement (Fig. 5b) only the first decay mode was used in order to minimize the background. The value of the asymmetry is $A = -.20\pm.13$, where -0.09 is expected.

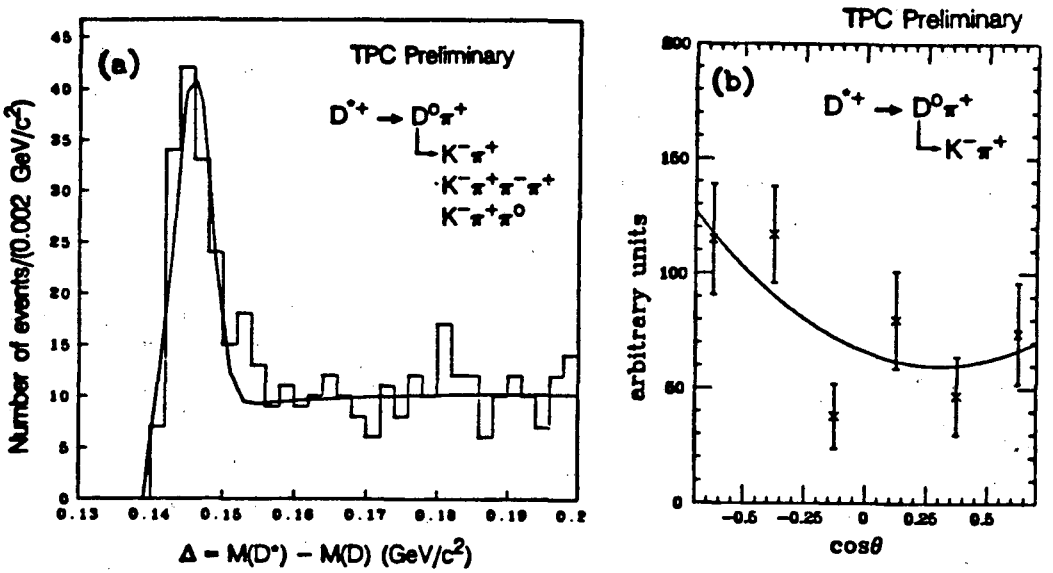

Fig. 5. TPC results on $D^{*\pm}$ production and asymmetry. (a) $D^{*+} - D^0$ mass difference (and c.c. states). The curve is a fit to a Gaussian shape (σ=3 MeV) and a smooth background. (b) Asymmetry for events with $D^0 \to K^-\pi^+$ (and c.c. states).

New results from HRS [11] on D^* production and asymmetry are shown in Fig. 6. Here no particle identification is used, the good momentum resolution ($\delta p/p$=0.1%p at high momentum) being sufficient to reduce backgrounds. The sample analyzed corresponds to 120 pb^{-1} of integrated luminosity. Figure 6a shows the mass difference for the $D^0 \to K^-\pi^+$ decay mode, with the requirement $z > 0.4$. Figure 6b shows the mass difference for another D^0 decay mode and Fig. 6d shows the asymmetry for the combination of three decay modes: $D^0 \to K^-\pi^+$, $K^-\pi^+\pi^0$, $K^-\pi^+\pi^+\pi^-$. The asymmetry from the whole sample is $A = -0.08 \pm 0.09$.

HRS [11] has also measured the asymmetry using inclusive $D^0 \to K^-\pi^+$ production. Because of the good momentum resolution, a D^0 peak is present in the $K\pi$ invariant mass (no particle identification is used), when the following two criteria are applied: i) require $|\cos\theta_K| < 0.7$, where θ_K is the angle between the kaon and the D direction in the $K\pi$ rest frame, ii) require $z > 0.5$. Table I shows the asymmetry obtained in this case; Fig. 6c shows the $K^-\pi^+$ (and c.c.) invariant mass distribution for the 120 pb^{-1} sample.

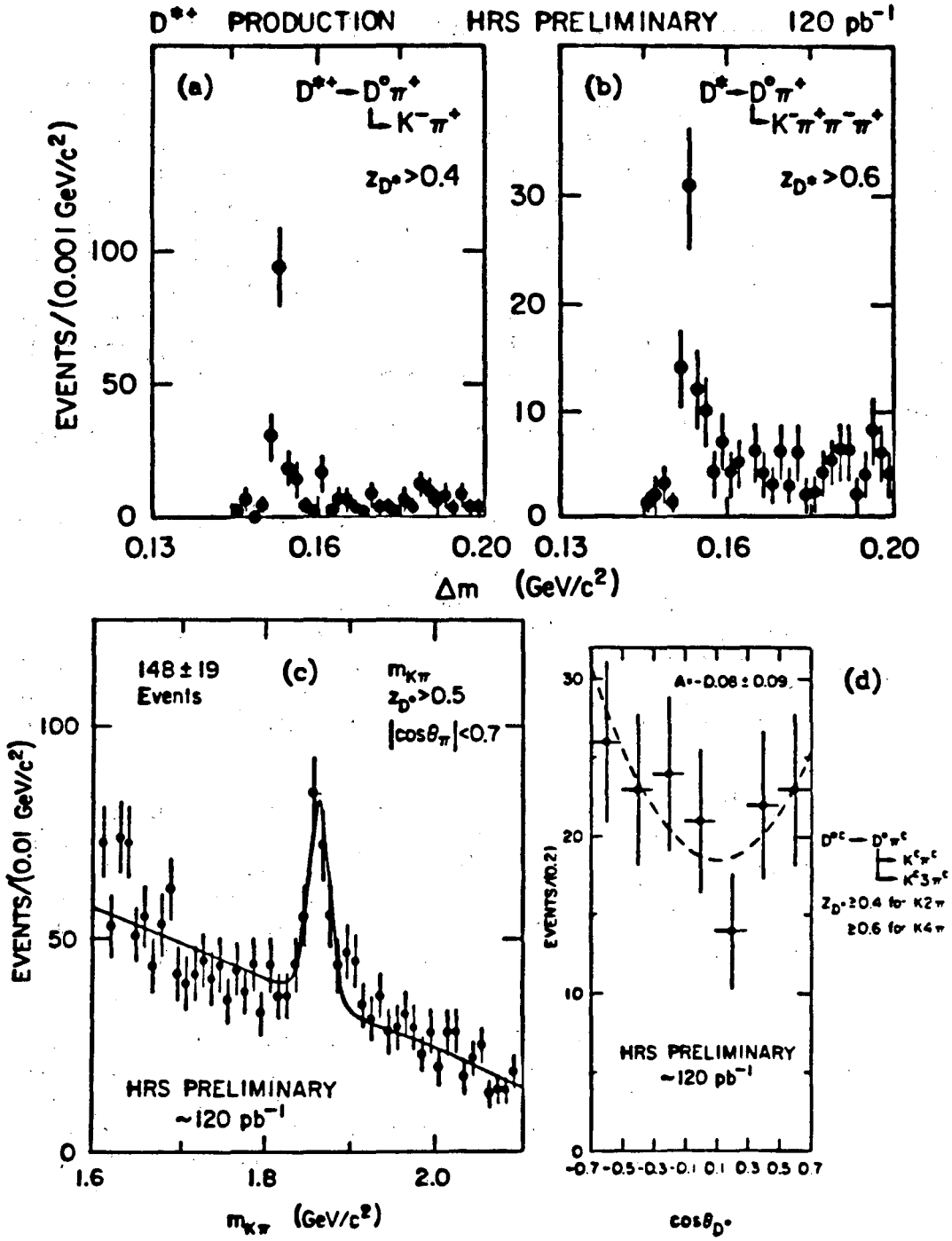

Fig. 6. HRS results on $D^{*\pm}$ production and asymmetry [11]. (a) $D^{*\mp}-D^{o}$ mass difference for $D^{o}\rightarrow K^{-}\pi^{+}$, (b) mass difference for the $D^{o}\rightarrow K^{-}\pi^{+}\pi^{+}\pi^{-}$ decay, (c) the $K^{-}\pi^{+}$ invariant mass distribution, and (d) asymmetry for the complete $D^{*\pm}$ sample.

3.2 Leptons as a Tag for b and c Quarks (TPC)

This method uses semileptonic decays of hadrons carrying charm or bottom quantum numbers to tag c and b quarks. The assumption is that the thrust axis of the jet containing the lepton gives the direction of the produced quark. In addition, the charge of the lepton is used to distinguish quark jets from antiquark jets. The expected asymmetry at $\sqrt{s}$ = 29 GeV (34 GeV) is −9% (−14%) for c quarks and −19% (−26%) for b quarks. The asymmetry is defined to be positive if there are more quarks than antiquarks produced along the direction of the incident electron.

There are various types of backgrounds to contend with:

a. Background due to hadrons misidentified as electrons or muons.

b. For the electron case, source of backgrounds are real electrons from γ conversion pairs (in the material between the e^+e^- interaction point and the tracking detector) and Dalitz pairs for which one of the electrons has too low a momentum to be detected.

c. Background from the other heavy quark. This is important because $c \rightarrow \ell^+$ whereas $b \rightarrow \ell^-$, so the background from the other quark will tend to reduce the asymmetry. It is therefore important to select c or b enriched samples and to estimate the contribution from the other heavy quark.

Two variables p and p_T with respect to the thrust or sphericity axis of the jets are used to separate the samples. In addition, an overall fit including as variables the semileptonic branching ratios, the z ($z=2E/\sqrt{s}$) distributions of the produced parent hadrons and the backgrounds has to be made before asymmetries are measured.

Many groups have published results using this technique [15–16]. New results come from TPC [17] which analyzed heavy quark decays into electrons. Electrons are identified by combining the information from the electromagnetic calorimeter (HEX) and the energy loss in the TPC. This allows a good hadronic

rejection. The hadron misidentification probability is 0.003%–0.3%, depending on p and p_T. The major source of background is due to electrons from photon conversions in the material (0.2 r.l) in front of the TPC. Figure 7 shows the electron spectra for the samples with $p_T < 1$ GeV/c and $p_T > 1.0$ GeV/c. Results of the overall fit to the data will be discussed in Sec. 4.1. For the asymmetry measurement, restricted samples have been chosen in order to reduce backgrounds. The c–enriched sample comprises 270 events with $p > 1.5$ GeV/c and $p_T < 1.0$ GeV/c; the b enriched sample includes 80 events with $p > 1.5$ GeV/c and $p_T > 1.0$ GeV/c. The contributions from $c \to e$ decays, $b \to c \to e$ decays, $b \to e$ decays and backgrounds are (57 ± 8)%, (7 ± 1)%, (12 ± 2)% and (24 ± 6)% in the c–enriched sample and (20 ± 3)%, (4 ± 1)%, (65 ± 6)% and (11 ± 3)% in the b–enriched sample, respectively. Figures 7c–d show the background subtracted and acceptance–corrected distributions of the angle between the incident e^- and the thrust axis. The results of the fits are shown in Table I.

3.3 Summary

Table I summarizes all the results obtained at PEP and PETRA. Here the systematic and statistical errors quoted by each experiment have been added in quadrature.

We notice the following;

a. values of $a_e a_c$ obtained from D^o, D^*, e and μ agree with each other.

b. If we assume $a_e = -1$ as expected we obtain for the average over all experiment the values:

$$a_c = 1.25 \pm 0.34 \qquad \text{Standard Model: } a_c = 1$$
$$a_b = -1.03 \pm 0.24 \qquad \text{Standard Model: } a_b = -1$$

In conclusion, the measured axial coupling constants for charm and bottom agree with the Standard Model predictions within ≅ 30%.

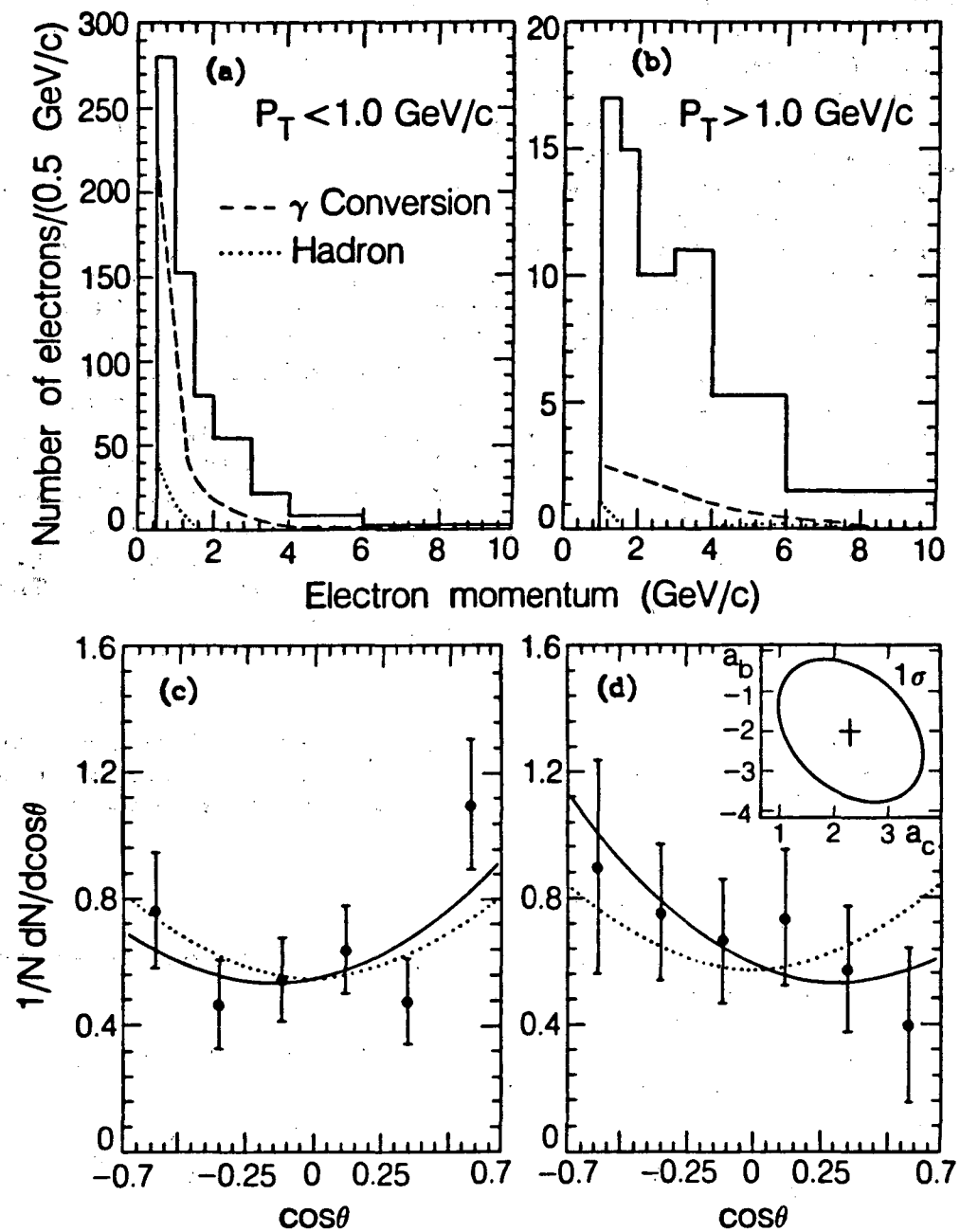

Fig. 7. TPC results on prompt electron spectrum and asymmetry [17]. (a), (c) charm enriched sample; (b), (d) bottom enriched sample. Dashed and dotted curves in (a), (b) show the background. Dotted curves in (c), (d) show the $1+\cos^2\theta$ distributions. The insert in (d) is the equal likelihood contour in the a_c–a_b plane.

Table I. Results on heavy quark axial coupling constants, for electrons, a_e and for b and c quarks, a_q. Here A is the measured asymmetry (see text).

Exp.	Quark	Ref.	$\sqrt{s}$ (GeV)	A (%) Measured	A (%) Expected	$a_e \cdot a_q$
	charm					
HRS	D*	11	29	-8±9	-9	-0.8±0.9
HRS	D^o	11	29	-11±14	-9	-1.2±1.3
TPC	D*	14	29	-20±13	-9	-2.1±1.4
TASSO	D*	11	34	-13±10	-14	-0.9±0.7
JADE	D*	12	34	-27±14	-14	-1.9±1.0
AVERAGE	D*					-1.21±0.43
TPC	e	17	29	(-22±16)[b]	-9	-2.3±1.7
MAC	μ	15	29	(-5±11)[a]	(-3)[a]	-1.6±3.6
MARK J	μ	16	35	-17±9		-1.2±0.6
AVERAGE	e,μ					-1.33±0.56
AVERAGE	charm					-1.25±0.34
	bottom					
TPC	e	17	29	(-38±37)[b]	-19	2.0±1.9
MAC	μ	15	29	(-7±9)[a]	(-12)[a]	0.6±0.7
MARK II	μ,e	15	29	(-28^{+13}_{-11})[b]	-19	$1.5^{+0.7}_{-0.6}$
MARK J	μ	16	35	-15±22	-25	0.6±0.9
TASSO	μ	16	34	-38±28	-27	1.4±1.0
JADE	μ	16	34	-26±9	-26	1.0±0.3
AVERAGE	bottom					1.03±0.24

a. Background not subtracted.
b. Derived quantity, not quoted by the authors.

4. HADRON PRODUCTION

Hadron production in e^+e^- collisions provides a simple source of jets that allow the study of the process of hadronization. The quark-parton model provides a simple explanation for the observed jet structure: e^+e^- annihilation first produces $q\bar{q}$ pairs which later fragment into hadrons producing the observed jets. The hadronization process, however, is not that simple; there are still a number of unanswered questions that need investigation. Detailed experimental information is essential.

Over the past few years a number of models have been developed to study the fragmentation of quarks and gluons into hadrons. In these models, quarks and gluons fragment into hadrons either "independently" from other partons [18], or in "color singlet strings" [19] or in "parton showers" based on perturbative QCD [20-22]. Some Monte Carlo generators using these different models have been made available to experimentalists and comparisons with data can be made. In this review the comparison will be mostly made with the LUND Monte Carlo [19].

In this section results obtained from PEP since the Cornell Conference [23] on heavy quark fragmentation, particle content of jets, baryon production and flavor correlations will be reported.

4.1 Heavy Quark Fragmentation

Direct information on heavy quark fragmentation is more accessible from the data than for light quarks. Tagging of heavy quarks can be done through D^*, D^0 and prompt leptons, as discussed in Sec. 3. Since the c and b quarks are heavy, $c\bar{c}$ and $b\bar{b}$ pairs are unlikely to be created in the hadronization process. The suppression factor is model dependent, but in first approximation it can be assumed that the heavy mesons will usually contain a first rank (primary) quark.

Experimental results have shown that the fragmentation function of heavy quarks is peaked at high energy. The heavy hadron is very likely to carry a large fraction ($z=2E/\sqrt{s}$) of the available energy. This was anticipated by Suzuki and Bjorken [24]. A simple form for the fragmentation function of heavy quarks has been suggested by Peterson et al. [25]

$$(4) \qquad D(z) = \frac{A}{z}\left(1-\frac{1}{z}-\frac{\varepsilon_Q}{(1-z)}\right)^{-2}$$

where A is a constant and $\epsilon_Q = m^2_q/m^2_Q$

Here Q and q indicate the heavy and light quark that make the heavy hadron. The experimental results are usually compared to this form.

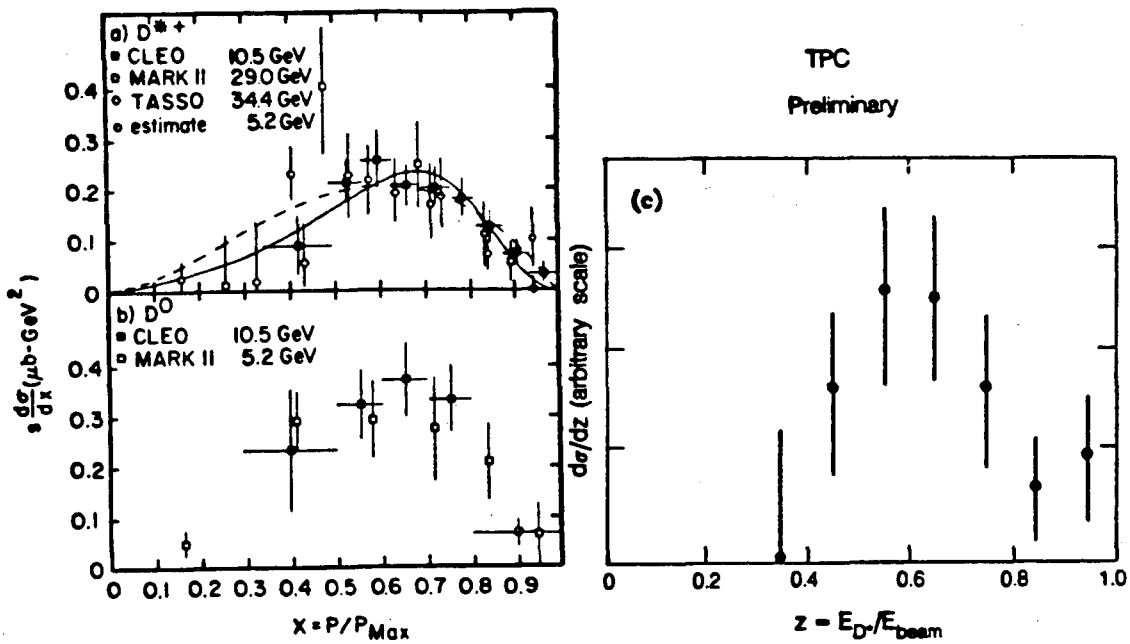

Fig. 8. Results on D^* fragmentation function. (a) Inclusive cross section as a function of x for D^{*+} as compiled by CLEO [10], including results from the MARK II [10] and TASSO [11]. (b) D^0 cross sections from CLEO [10] and MARK II [26]. (c) The TPC preliminary data on D^* fragmentation [14].

A. Charm fragmentation from D^* (TPC). New results on D^* fragmentation are reported by TPC [14]. The $D^{*+}-D^0$ mass difference is shown in Fig. 5 and details are given in Sec. 3.1. The fragmentation function is shown in Fig. 8c. A partial compilation of results from other experiments, on D^* and D^0 is shown in Fig. 8a,b taken from Avery et al. [10]. Here data from CLEO [10], TASSO [11], MARK II at 29 GeV [10], and MARK II at 5.2 GeV [26] are shown in a plot of the scaled cross section $s d\sigma/dx$. Values of $\langle z \rangle$ and of ϵ are shown in Table II. All data agree within errors.

B. Results from prompt leptons (TPC, DELCO). As discussed in Sec. 3.2, the prompt leptons in hadronic events can be used as tag of c and b quark fragmentation into hadrons. From the lepton spectrum it is possible to infer the spectrum of the hadrons produced from heavy quarks and measure their z distributions.

New results from PEP are from DELCO(e) [27] and TPC(e,μ) [17,14]. The TPC electron identification and data have been discussed in Sec. 3.2. In the DELCO experiment, electron identification is made primarily with a threshold Cerenkov counter, although extra rejection of background is done with a shower counter. Two separate experiments were carried out by filling the Cerenkov counter with isobutane (range 0.5 to 2.5 GeV/c) and then with nitrogen (range 0.5-5.5 GeV/c). Results from the two experiments agree within statistics. Backgrounds to the electron signal are due mostly to γ conversions and misidentified hadrons (total of 28% and 18% for the two different experimental conditions). Figure 9a shows the electron cross section for the DELCO measurements along with those for TPC [17] and MARK II [15]. Figure 9b shows the DELCO background substracted p_T distribution. This illustrates how effective the cut at P_T = 1 GeV is in separating the charm enriched from the bottom enriched samples.

The TPC muon results [14] are shown in Fig. 10. The TPC muon system covers 98% of the solid angle with four layers of proportional chambers and a total iron thickness varying between 0.67 and 1.25 meters of steel. For this analysis only part of the solid angle is used and the muon momentum cutoff is at 2 GeV/c. The background from kaon decays is reduced by using the dE/dx particle identification in the TPC. The sample of 982 muon candidates includes a background from punch-through and decays of 38%. Figure 10 shows the background subtracted c and b enriched samples.

The results obtained by the different groups are summarized in Table II. The procedure used is to make an overall fit to the data in bins of p and p_T (including background) with four free parameters: semileptonic branching ratios for b and c quarks, ϵ_c and ϵ_b (see Eq. 4). From the values of ϵ one can then calculate the <z> for each quark. Both ϵ and <z> are reported in Table II.

C. Summary. Many experiments have measured heavy quark fragmentation parameters. They are summarized in Table II. The results are in good agreement within errors in the measured values of <z>. The values of ϵ show a larger variation, but, since D(z) varies slowly with ϵ, this does not imply a variation in shape between the many experiments.

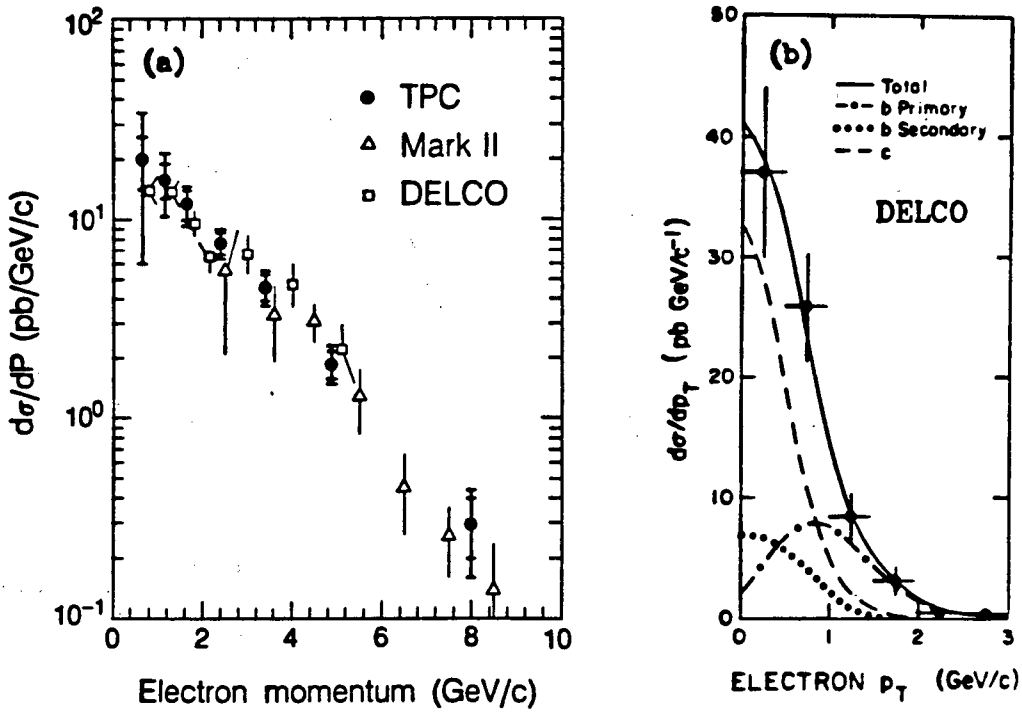

Fig. 9. (a) Prompt electron spectrum from the TPC [17], DELCO [27] and MARK II [15]. (b) DELCO's background subtracted p_T distribution of direct electrons. Curves represent different contributions to the spectrum.

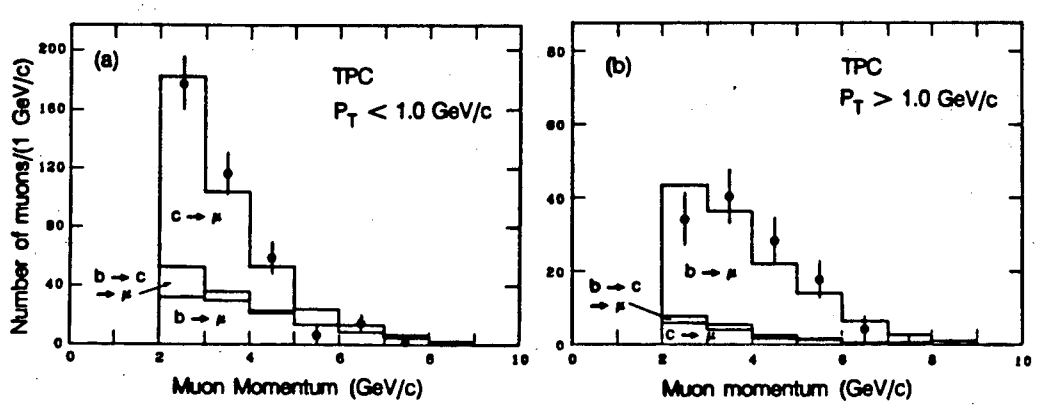

Fig. 10. TPC background subtracted spectra of direct muons (preliminary) [14]. (a) Charm-enriched sample, (b) bottom-enriched sample. The different contributions to the spectrum shown are the result of a fit.

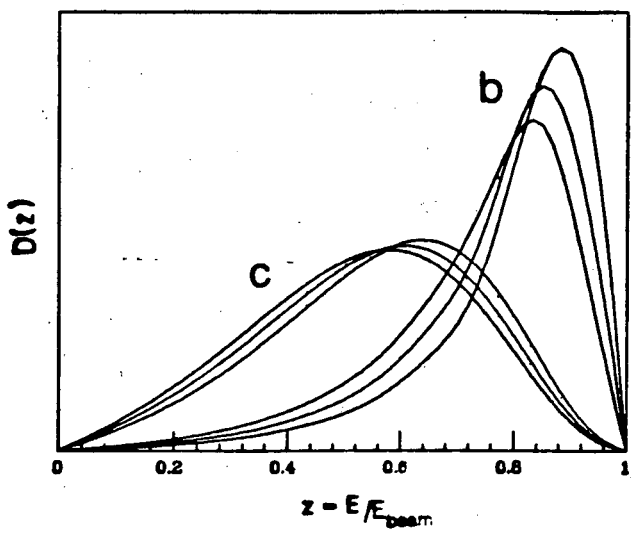

Fig. 11. The Peterson et al. [25] form for the charm and bottom fragmentation function, calculated with $\epsilon_c=0.25\pm0.05$ and $\epsilon_b=0.017\pm^{0.010}_{0.007}$ (see text).

Can the results from the different experiments be averaged? This seems to be somewhat inappropriate because some experiments, i.e. MARK J [29] and MAC [15], use a different variable $z = (E+p_L)/(E_Q+p_Q)$, rather than $2E_h/\sqrt{s}$. TASSO [29] used both and gave results for c and b quarks that differ by (5-8)% for the two parameterizations. Another difficulty is due to radiative corrections: DELCO quotes two values (with and without radiative corrections) that differ by (2-4)%. With caution then, we can average the results. For charm we average $\langle z\rangle_c$ as obtained from the D^* data, without including the CLEO results, because the value of z_{min} is very different from the others. This average (see Table II) agrees very well with the average from the e, μ data. For ϵ_c we also average the D^* data. For the bottom quark, the errors on the measured ϵ_b are very asymmetric, so we choose to average $\langle z\rangle_b$ and derive ϵ. The results are as follows:

$$\langle z\rangle_c = 0.57\pm0.01 \qquad \epsilon_c = 0.25 \pm 0.05$$

$$\langle z\rangle_b = 0.78\pm0.03 \qquad \epsilon_b = 0.017 \pm 0.010$$

the errors are the ones obtained in the weighted

Table II. Heavy quark fragmentation results, from e^+e^- experiments. In all cases systematic and statistical errors have been added in quadrature for this summary. Average values to be taken with caution (see text).

		$\sqrt{s}$	$\langle z \rangle$[a]	ε	Ref.
	Charm				
MARK II	D*	29	0.58±0.06		10
CLEO	D*	10.5	[0.63±0.02][b]	[0.10±0.02][b]	10
TASSO	D*	34.4	0.58±0.04	0.18±0.07	11
HRS	D*	29	0.56±0.02	0.29±0.10	28
HRS	D^0, D^+	29		0.36±0.12	28
TPC	D*	29	0.58±0.02	0.28±0.11	14
Average	D*		0.57±0.01	0.25±0.05	
MARK J	μ	34.6	0.46±0.05	(0.80±0.22)[c]	28
TASSO	μ	34.4	$0.71^{+0.06}_{-0.13}$	$0.006^{+0.055}_{-0.006}$	29
TASSO	e	34.4	$0.55^{+0.11}_{-0.09}$	$0.23^{+0.39}_{-0.18}$	30
TPC	μ	29	0.55±0.08	$0.26^{+0.30}_{-0.14}$	14
DELCO	e	29	0.66±0.06	$0.071^{+0.076}_{-0.038}$	27
Average	μ,e		0.56±0.03		
	Bottom				
MARK II	e	29	0.79±0.09	$0.015^{+0.032}_{-0.016}$	15
MARK II	μ	29	0.73±0.18	$0.043^{+0.235}_{-0.054}$	15
MARK J	μ	34.6	0.75±0.07	(0.15±0.06)[c]	28
MAC	μ	29	0.80±0.10	$0.008^{+0.037}_{-0.008}$	15
TASSO	μ	34.5	$0.81^{+0.05}_{-0.10}$	$0.0025^{+0.0310}_{-0.0028}$	29
TASSO	e	34.5	0.75±0.08	$0.022^{+0.042}_{-0.020}$	30
DELCO	e	29	0.76±0.06	$0.025^{+0.034}_{-0.015}$	27
TPC	μ	29	0.83±0.06	$0.0065^{+0.0204}_{-0.0042}$	14
TPC	e	29	0.74±0.06	$0.033^{+0.042}_{-0.023}$	17
Average Bottom			0.78±0.03	$(0.017^{+0.010}_{-0.007})$[d]	

[a] All experiments, except MARK J and MAC, use $z=2E_h/\sqrt{s}$ (see text).
[b] Values not included in the average.
[c] This is the quoted value for $\sqrt{\varepsilon}$.
[d] Value obtained from $\langle z_b \rangle$.

average and do not reflect the problems discussed above. So these values are used only to show qualitatively the difference between the two fragmentation functions (Fig. 11). The best way to obtain an average would be to fit all the data together, rather than average the individual results.

4.2 Inclusive Particle Production

Two types of data can be obtained by studying production of different particles in jets: particle yields and particle spectra.

Particle yields provide information on multiplicities of $q\bar{q}$ pairs pulled from the vacuum, on the type of pairs (i.e. u:d:s ratio), on the ratio of diquark to quark pairs (relevant to one model of baryon production) and also on how many vector-vs-pseudoscalar particles (V/P ratio) are produced in the hadronization phase.

Particle spectra provide information on the fragmentation function, D(x). The spectra are usually presented in distributions like

$$D(x) = (1/\sigma\beta)\ d\sigma/dx$$

with $x = 2E_h/\sqrt{s}$ (different variables are used by different experiments, $x_p=2p/\sqrt{s}$ is often used) and β is the velocity of the particle. D(x) represents then the probability that a particle is produced at x in a unit interval of x.

In this section new results on single particle production and on resonance production will be presented.

A. Single Particle Production (HRS,TPC). A large fraction of the particles produced in a jet are pions that are mostly decay products of resonances. The charged pion multiplicity has been measured by TASSO [31] and now by TPC [32] to be about 10.5 out of 13 charged particles. New results discussed here are on charged particles (HRS [33] and TPC [32]), on γ and π^o production (TPC [14]), and on Λ and Ξ (TPC [14]).

Figure 12a shows the HRS inclusive charged particle spectrum (obtained in a sample of $\int Ldt=20pb^{-1}$) compared with earlier results from TASSO

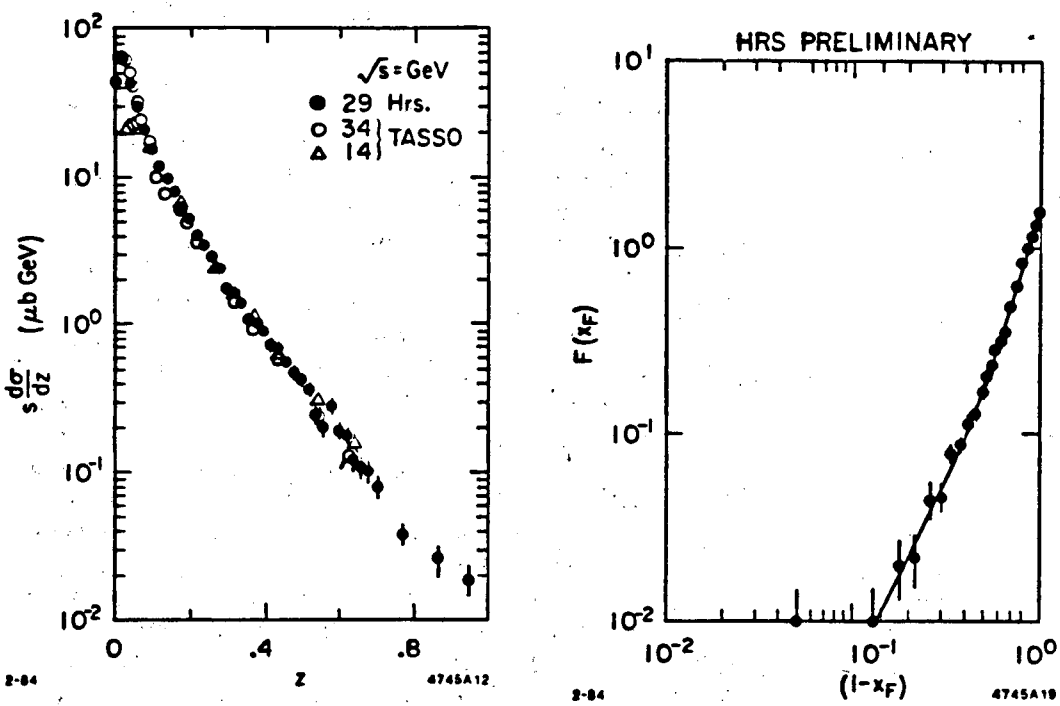

Fig. 12. Inclusive cross sections for charged hadron production measured by HRS [33]. (a) Scaled cross section versus $z=2p/\sqrt{s}$, compared with TASSO [34], (b) same data plotted in terms of $x_F=2p_L/\sqrt{s}$, p_L being the momentum component along the thrust axis. The vertical axis is $F(x_F)=(1/\sigma\pi)(2E/\sqrt{s})(d\sigma/dx_F)$.

[34] at 14 and 34 GeV. The agreement is very good in the overlap region. The HRS data extend to higher z values. The same data are shown in Fig. 12b, plotted in a variable more appropriate to study longitudinal fragmentation properties. The variable is $x_F = 2p_L/\sqrt{s}$, where p_L is the component of the momentum of the particle along the thrust axis. The data suggest a flattening off of the spectrum at large values of x_F that the authors attribute to production of hadrons from light quarks. Monte Carlo studies indicate that hadrons that are decay products of particles containing heavy quarks contribute mostly in the region with $x_F < 0.6$. The curves represent separate fits to the data in the ranges $x_F=0.1$ to 0.6 and $x_F=0.6$ to 0.9 to the function $(1-x_F)^n$. Values of $n = 3.36 \pm 0.01$ and $n = 2.16 \pm 0.35$ were obtained for the two regions. These values of n support the hypothesis that light quarks are the major contributors at large x. Another question that HRS may be able to answer with their full sample of data is the behavior for

$x \to 1$, a region that so far has been inaccessible to other experiments.

TPC has recently published the normalized cross sections versus x for $\pi^{\pm}$, $K^{\pm}$, p and $\bar{p}$ [32]. The dE/dx measurements of the TPC (Fig. 13) are used to identify particles in jets. At low momentum simple counting in the π,K,p, bands will provide the number of particles of the different species. In the region of ambiguity with the electron band, electron subtraction is done by estimating the electron contamination by smooth fits to the spectrum outside the region of ambiguity. In the relativistic rise region the electron subtracted spectrum is fit to a sum of three distributions (for π,K,p) by maximum likelihood method (see inset in Fig. 13). The final corrected distributions for the three types of particles are shown in Fig. 14. The curves are calculated using the LUND model [19]. The baryon production mechanism included in this model assumes that a fraction of the times a diquark anti-diquark pair is produced in the color field rather than a quark antiquark pair. The diquark pair then combines with a quark to form a baryon. The parameters used are as follows: s/u probability ratio, P(s)/P(u)=0.3, and diquark to quark probability, P(qq)/P(q)=0.09. The integrated distributions give the following multiplicities:

$$N = 10.7 \pm 0.6$$
$$N^{\pi\pm} = 1.35 \pm 0.13$$
$$N^{K\pm} = 0.60 \pm 0.08$$
$$N_{p,\bar{p}}$$

The preliminary inclusive π^{o} differential cross section from the TPC [14] is shown in Fig. 15a. The electromagnetic calorimeter (HEX) [35] of the TPC facility consists of six modules, outside the 1.4 r.l. conventional magnet coil. Each module consists of 40 layers of lead-fiberglass-aluminum laminates with gold-plated tungsten wires in the 6 mm thick gas gap. It operates in Geiger discharge mode, in a 1 atm argon ethyl-bromide (4%) gas mix. The photon energy resolution is 16% at 1 GeV. Photons can also be reconstructed from γ conversion pairs in the 0.2 r.l. of material ahead of the TPC. The two spectra agree with each other within errors. Photons from the HEX are used to reconstruct π^{o}s at momenta $P_{\pi o} > 1$ GeV/c.

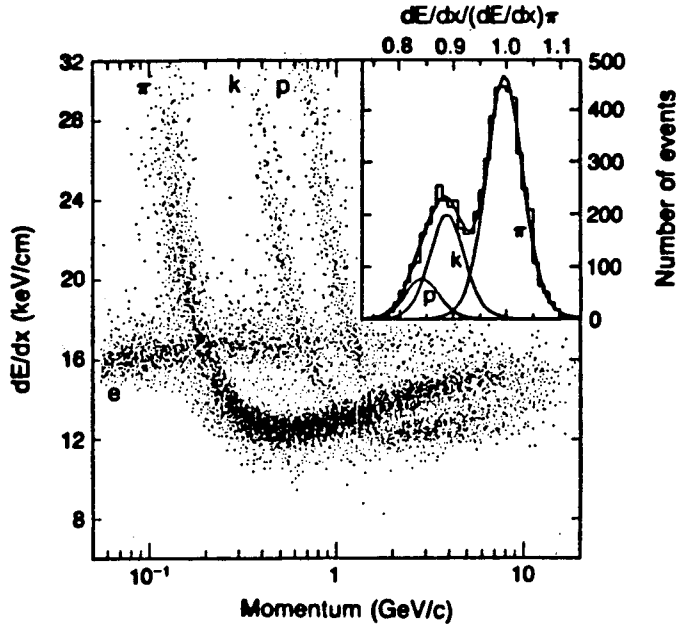

Fig. 13. The TPC dE/dx measurement versus momentum [32]. Clean bands for π, K, p are seen. The inset shows the ratio to the dE/dx expected for pions, for tracks with $3.5<p<6.0$ GeV/c.

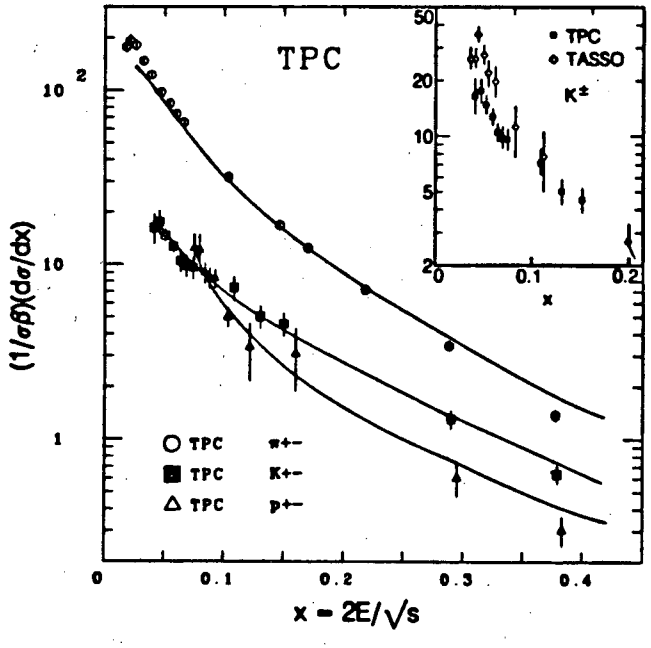

Fig. 14. TPC normalized cross section versus x for pions, kaons and protons at $\sqrt{s}$=29 GeV [32]. The inset shows the comparison with TASSO [31]. The curves are calculated using the LUND Model.

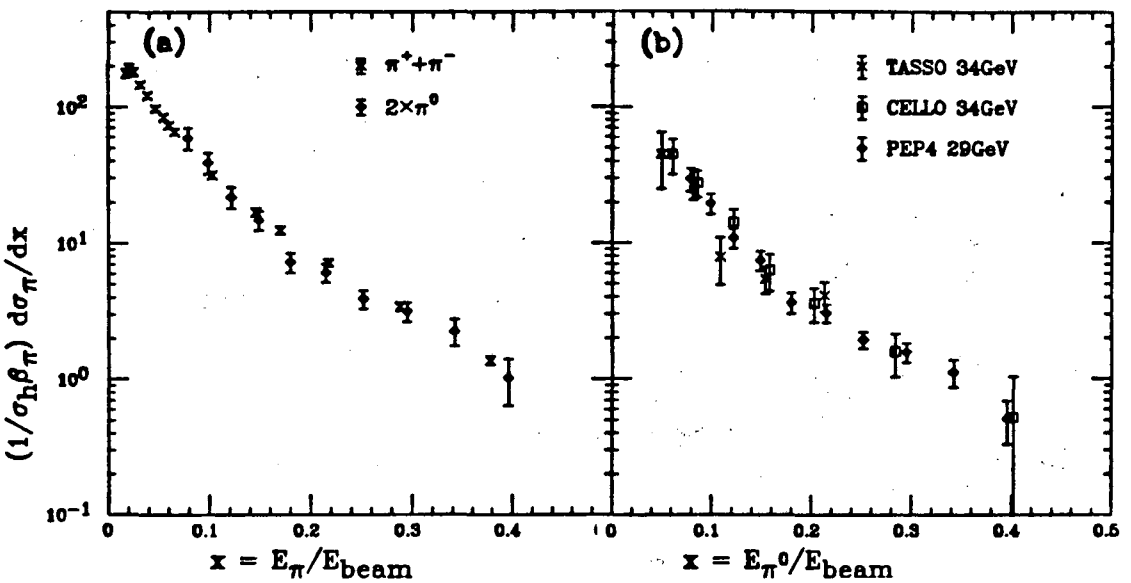

Fig. 15. Neutral pion normalized cross section measured by the TPC [14]. (a) Comparison with TPC charged pion data [32]. (b) Comparison with TASSO [36] and CELLO [37].

The measured π^o spectrum, compared with TASSO [36] and CELLO [37] is shown in Fig. 15b. The comparison with TPC's measured charged pion spectrum [32] is shown in Fig. 15a. The ratio $2\sigma(\pi^o)/(\sigma(\pi^+) + \sigma(\pi^-)) = 0.92 \pm 0.14$ indicates a very good agreement between the two spectra. The total energy going into photons is measured to be E_γ=7.4±0.7 GeV. The neutral pion energy is E_{π^o}=6.2±0.8 GeV, to be compared with the charged pion energy of $E_{\pi^\pm}$=12.1±0.7 GeV. The measured π^o multiplicty (integrated over the whole spectrum) is found to be N_{π^o}=5.3±0.7 to be compared with $N_{\pi\pm}$=10.7±0.6 discussed above.

The TPC Collaboration also reports results on Λ and Ξ production [14]. TASSO first observed Ξ production with a sample of 14 events [38]. The TPC results are shown in Fig. 16. The Λ sample (Fig. 16a) selection criteria are based on kinematics of the Λ decay into $\pi^- p$, on flight distance and on requirements that the dE/dx measurements (Fig. 13) for the pions and protons are consistent with the expected values for the assigned mass hypothesis. The detection efficiency for Λ reaches a maximum of 15% at 2 GeV/c and decreases to several per cent at 10 GeV/c. A

total of 570 Λs and $\bar{\Lambda}$s are obtained. The Ξ sample was selected with criteria based on kinematics of the $\Xi \rightarrow \Lambda\pi$ decay, for a momentum $P_{\Xi} > 1$ GeV/c, and on identification of the pion by dE/dx measurement. The efficiency was about 2%. Figure 16b shows the Ξ^- signal of 16±4 events, the curves show the result of a fit with a smooth background and a Gaussian (σ=18.7±4.3 MeV). The shape of the background was obtained by fitting the sample of "wrong sign combinations," i.e., $\Lambda\pi^+$ and $\pi^-\bar{\Lambda}$ events (not shown).

Figure 16c shows the differential cross sections for protons, lambda and Ξ^- as measured by the TPC. The curves are again obtained with the LUND model [19]. The values of the relevant parameters are:

$$R = P(qq)/P(q) = 0.085$$
$$r = (P(su)/P(ud))*(P(d)/P(s))=0.4$$

where P(qq) and P(q) are the probabilities to produce a diquark or a quark pair, respectively. For r, the extra strange-diquark suppression factor, the flavors are explicitly indicated. The values of these parameters are different from the default values of the LUND program (R=0.09, r=0.2), but they are not the result of an overall fit. Particle yields obtained by integrating the distributions of Fig. 16c over the entire energy region, are

$$N_{p,\bar{p}} = 0.60 \pm 0.08$$

$$N_{\Lambda,\bar{\Lambda}} = 0.216 \pm 0.013 \pm 0.018$$

$$N_{\Xi,\bar{\Xi}} = 0.025 \pm 0.009 \pm 0.006$$

where both statistical and systematic errors are included (for the first measurement the two errors have been added in quadrature). The Λ and Ξ results are in agreement with the TASSO results [38], shown in Table III.

B. Resonance Production (MARK II, TPC, DELCO). The investigation of resonance productin in e^+e^- annihilation provides important information on parton fragmentation. Most of the single particles we have discussed in the previous paragraphs are decay products of resonances, and therefore they are one more step removed from the original partons. The fraction of vector mesons produced, V/P ratio, is an

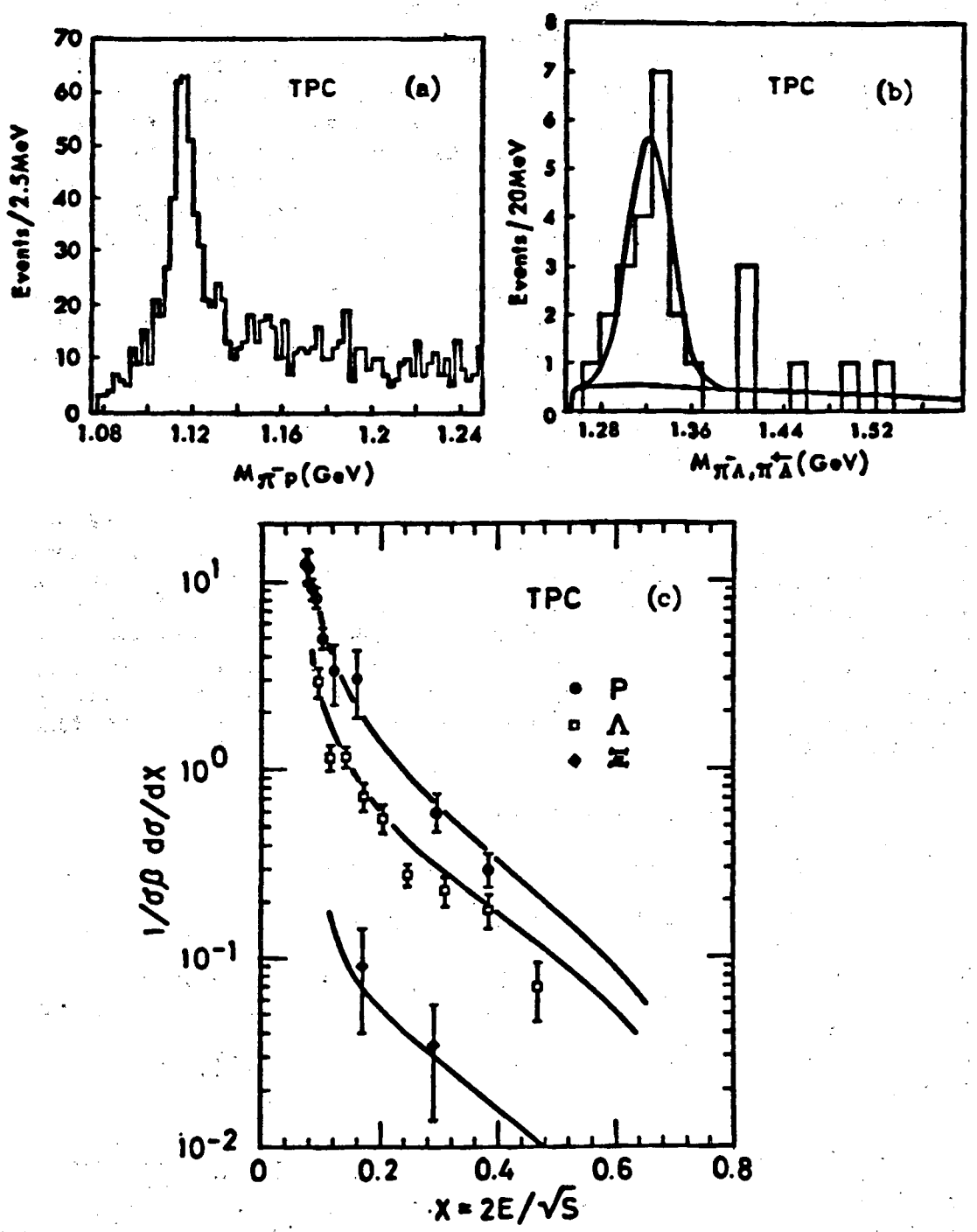

Fig. 16. Inclusive Λ and Ξ production (TPC, prelim.). (a) The $\pi^- p$ invariant mass showing the Λ signal, (b) the $\Lambda\pi^-$ (and c.c.) spectra showing the Ξ signal, and (c) inclusive p, Λ, Ξ cross sections. The curves are from the LUND Model.

important parameter in many models [18-22], therefore, it is important to determine it from the data. In addition, the mass spectrum of hadrons produced in the hadronization process can be approximately predicted in some models and therefore it is important to try to measure it.

New results on ρ and K^* production are reported by MARK II [39], on K^* and ϕ production by TPC [14,40] and on ϕ production by DELCO [41].

The MARK II data [39] used to study ρ^o and K^{*o} production are shown in Fig. 17. No particle identification is used, so each track is considered alternatively to be a pion or a kaon. All possible $\pi^+\pi^-$ pairs are plotted in Fig. 17a; all possible $K^\pm\pi^\mp$ pair are shown in Fig. 17b. The $\pi\pi$ plot includes contributions from K^{*o} where the $K^\pm$ has been misidentified as a pion. The $K\pi$ plot includes contributions from K_s, ρ, ω where one of the pions has been misidentified as a kaon, as well as contribution from K^{*o} where the K and π are given the wrong mass assignment. Using only pairs with P > 1 GeV/c, a simultaneous fit to both distributions was made, adding contributions from background (a 4th order polynomial), K_s, ω, ρ and K^*. The shapes for these states are those obtained from Monte Carlo; the normalizations are left free. After background subtraction, the results are shown in Fig. 17c,d, where each contribution is drawn separately. The ρ^o and K^{*o} yields were obtained from this fit to be N_ρ = 6255±780, N_{K^*}=3635±565. After acceptance correction for each state they obtain

$$\sigma(K^*)/\sigma(\rho) = 0.87 \pm 0.18 \pm 0.22$$

The number of ρ and K^* per event are:

$$N_\rho = 0.410 \pm 0.051 \pm 0.067 \quad \text{for} \quad 0.07<x<0.7$$

$$N_{K^*} = 0.356 \pm 0.056 \pm 0.095 \quad \text{for} \quad 0.07<x<0.7$$

where the first error is from statistics, the second from systematics. The ρ^o differential cross section, shown in Fig. 17e, agrees with earlier measurements by TASSO [42]. The TASSO yield/event shown in Table III, is integrated over the whole x range.

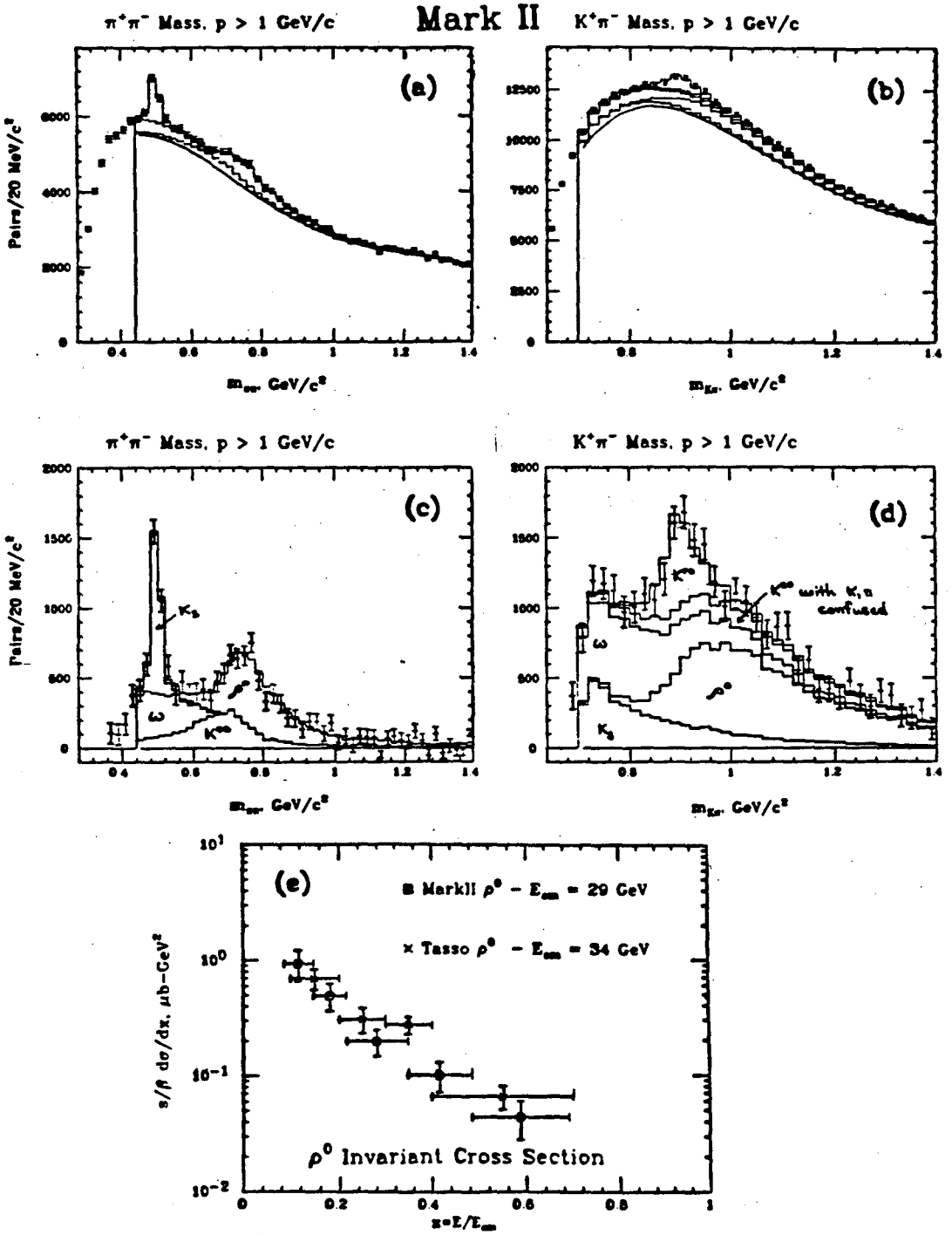

Fig. 17. Inclusive ρ and K^{*0} production reported by MARK II [39]. (a), (b) $\pi^+\pi^-$ and $K^+\pi^-$ spectra respectively; (c) and d), as (a) and (b), with background subtracted. (e) Inclusive ρ^0 cross section versus x, compared with TASSO [42].

The TPC results on K^* and ϕ production [14,40] are shown in Fig. 18. Here particle identification is used and the resonances appear as peaks in the $K^-\pi^+$ and K^+K^- invariant mass, respectively. The kaons are identified unambiguously at low momenta (Fig. 13). At other momenta and in the overlap regions a method based on the probability that a track be a kaon is used [40]. From the measured dE/dx and momentum for each track and the empirically determined dE/dx curves for each particle type ($i = e,\pi,K,p$) a χ^2 is calculated for each track hypothesis. A probability for the track to be of type i is calculated from the χ^2, and then weighted by the measured charged particle fractions [32] as function of momentum. A probability $w > 70$ % is then required for a kaon to be identified, assuring a purity of 70% on the average for the kaon sample. For the K^* analysis, a similar procedure is also used for the pion identification.

In a 69 pb^{-1} sample of data analyzed this way the $K\pi$ and KK invariant mass plots of Fig. 18a-c are obtained. Fits with the sum of a Breit-Wigner shape and a smooth background to the "unlike signs" distributions yield 2250±120 K^* events and 62±11 ϕ events. The r.m.s. width for the ϕ peak in Fig. 18b is 6.2±0.4 MeV, consistent with the detector resolution. The normalized inclusive cross sections versus x ($2E/\sqrt{s}$) for K^* and ϕ production are shown in Fig. 18e. The TPC results for K^* (preliminary) [14] and for ϕ [40] produced per event are as follows:

$$N_{K^*} = 0.39 \pm 0.04 \pm 0.05 \qquad 0.1<x<0.8$$

$$N\phi = 0.084 \pm 0.013 \pm 0.018 \qquad 0. <x<1.$$

The curves shown have been calculated with the LUND model [19] using $s/u = 0.3$ and $V/P = 1$. They agree with the data reasonably well.

The DELCO results on ϕ production [41] are shown in Figs. 18d and 18e. A sample of 92 pb^{-1} of data has been used. The kaons are identified above 2.5 GeV/c by a Cerenkov counter filled with isobutane with pion threshold at 2.5 GeV/c. Figure 18d shows the invariant K^+K^- mass distribution obtained when both tracks are identified by the Cerenkov counter. An enhancement is observed at the ϕ mass, containing 26 ϕ with an estimate background of 14 events. The width of the peak is σ=10 MeV, consistent with the

Table III. Particle yield measured at PEP and PETRA in e^+e^- Collisions in the $\sqrt{s}$ = 29-34.5 GeV range.

Particle	Particles/Event	Experiment	Ref.	Remarks
$\pi^\pm$	10.7 ±0.6	TPC	32	
	10.3 ±0.4	TASSO	31	
π^0	6.1 ±2.0	TASSO	36	
	5.2 ±1.8	CELLO	37	
	5.3 ±0.7	TPC	14	
η	0.72±0.10±0.18	JADE	46	
ρ^0	0.73±0.06	TASSO	42	
	0.410±0.051±0.067	MARK II	39	x=0.1-0.7[a]
$K^\pm$	1.35±0.13	TPC	32	
	2.0 ±0.2	TASSO	31	
$K^0+\bar{K}^0$	1.6 ±0.1	TASSO	43	
	1.45±0.08±0.15	JADE	44	
$K^{*0}+\bar{K}^{*0}$	0.39±0.04±0.05	TPC	14	x=0.1-0.8
	0.356±0.056±0.095	MARK II	39	x=0.07-0.7
ϕ	0.084±0.013±0.018	TPC	40	
D^0	(0.48±0.17)[b]	HRS	11	x > 0.5
D^+	(0.21±0.09)[b]	HRS	11	x > 0.5
$D^{*\pm}$	0.31±0.08±0.11	TASSO	11	x > 0.3
$D^{*\pm}$	(0.25±0.09)[b]	HRS	11	
$F^\pm$	(0.015±0.003±0.005)/B	TASSO	45	x>0.3 B=BR($F\to\phi\pi$)
$p+\bar{p}$	0.60±0.08	TPC	32	
	0.8 ±0.1	TASSO	31	
$\Lambda+\bar{\Lambda}$	0.216±0.013±0.018	TPC	14	
	0.28±0.04	TASSO	43	
Ξ^-	0.025±0.009±0.008	TPC	14	
	0.026±0.008±0.009	TASSO	38	

[a]In this x interval the TASSO result agrees very well with the MARK II.

[b]Calculated by us, using R_h = 4.0.

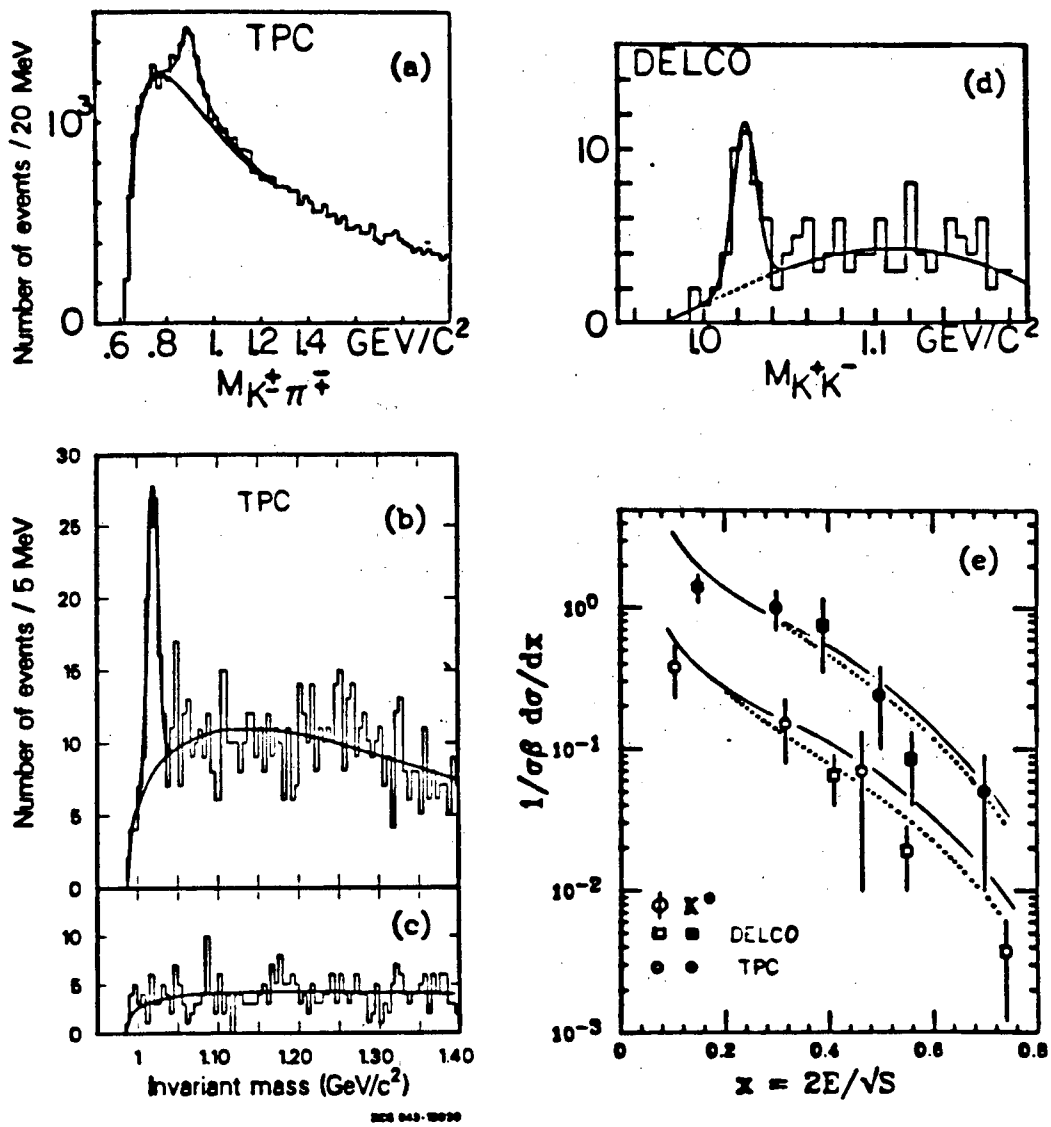

Fig. 18. Vector meson production data. (a) $K^\pm\pi^\mp$ invariant mass from the TPC [14]. (b) and (d) K^+K^- invariant mass from the TPC [40] and DELCO [41] respectively. (c) Same charge KK mass distribution from the TPC. (e) Normalized inclusive cross sections for K^* and ϕ production. The curves are calculated with the "Symmetric" LUND Model (solid lines) and with the "Standard" LUND Model (dashed lines).

resolution. The region of x covered is $0.35<x<0.8$. The values obtained for the normalized cross section are plotted in Fig. 18e and are in agreement with the TPC data.

C. Summary. New results on single particle and resonance production from PEP add information to the wealth of data collected so far in e+e- annihilation on jet production.

Table III is a compilation of the published measurements on particle yields and the new results presented here on $K^{\pm}$, $\pi^{\pm}$, π^{o}, p, Λ and Ξ. Information on resonant states is particularly important because resonances are more directly related to the quantum numbers and the production mechanisms of the original partons. The new results reported here on ρ^{o}, K^{*o} and ϕ production are also included in Table III.

The inclusive x distributions for charged particles reported by HRS (Fig. 12) shows a flattening off at large x, providing more information on light quark fragmentation. The x distributions for charged particles reported by the TPC (π,K,p,Λ,Ξ in Figs. 14 and 16) are in agreement with expectations from the LUND Model with parameters

$$u/s = 0.3 \qquad qq/q = 0.085$$
$$V/P = 1 \qquad (sd/ud)*(d/s) = 0.4$$

The LUND Model [19] also agrees well with the K^{*o} and ϕ distributions from the TPC, shown in Fig. 18.

4.3 Characteristics of Proton Production in Jets (TPC).

Baryon production in quark and gluon fragmentation provides important information for the study of jet formation. Baryons, because of their large mass, experience little momentum degradation in resonance decays, thus they carry information that closely reflects the distribution of primary fragmentation products.

The TPC group has done a detailed study of proton production [47]. The data are shown in Fig. 19. Figure 20a shows the TPC measured fraction [32] of different charged particle species in jets at $\sqrt{s}$ = 29 GeV. The general trend is that at high momentum the

kaon and proton fractions (f_K and f_p respectively) increase, whereas the pion fraction decreases. This is well described by the LUND Model [19]. The increase of f_p with momentum is shown in more details in Fig. 19a, where now the "Standard" LUND is used with the value qq/q = 0.075. The dependence of f_p on p_T, transverse momentum to the sphericity axis, is shown in Fig. 19b-e for different ranges of total momentum p. Here again a sharp increase with p_T is observed. The same effect has been observed by the EMC collaboration in deep inelastic lepton-nucleon scattering [48]. For momenta above 3.7 GeV/c the p_T dependence flattens out.

The high value of f_p at large p_T and the large f_p seen in T decays [49] has stimulated speculations that proton production increase is related to gluon emission [50]. The TPC results can be explained with an alternative mechanism, higher proton production in gluon jets not being necessary to explain the data [47]. The alternative mechanism is simply that f_p is constant at the level of primary produced hadrons and the apparent increase in f_p with p and p_T is due to the effects of resonance decays. Resonances produce a large number of low energy pions that dilute the proton fraction in jets. The dashed lines in Fig. 19 show the fraction of protons among the primary hadrons as calculated by the "Standard" LUND Model. Here f_p appears to be constant with p_T, whereas among all the particles (solid line) f_p has a strong p_T dependence. Only at large values of p (Fig. 19e), where resonance decay effects are suppressed, the flat p_T dependence survives.

Another aspect of proton production studied by the TPC group is the p_T distribution of protons at a fixed rapidity. Figure 20b shows the proton cross section $(1/\sigma)d\sigma/(dydp_T^2)$ for the $|y|<1$ region. The corresponding pion cross section is also shown for comparison. The proton p_T distribution can be represented by a Gaussian shape with $\sigma = 0.55 \pm 0.04$ GeV/c. The full lines represent the prediction of the LUND Model that has been tuned to describe the mean p_T of the observed mesons. It reproduces the large p_T of the protons with no additional assumptions. The protons are likely to reflect the p_T distribution of primary hadrons, whereas resonance decays soften the observed pion distributions.

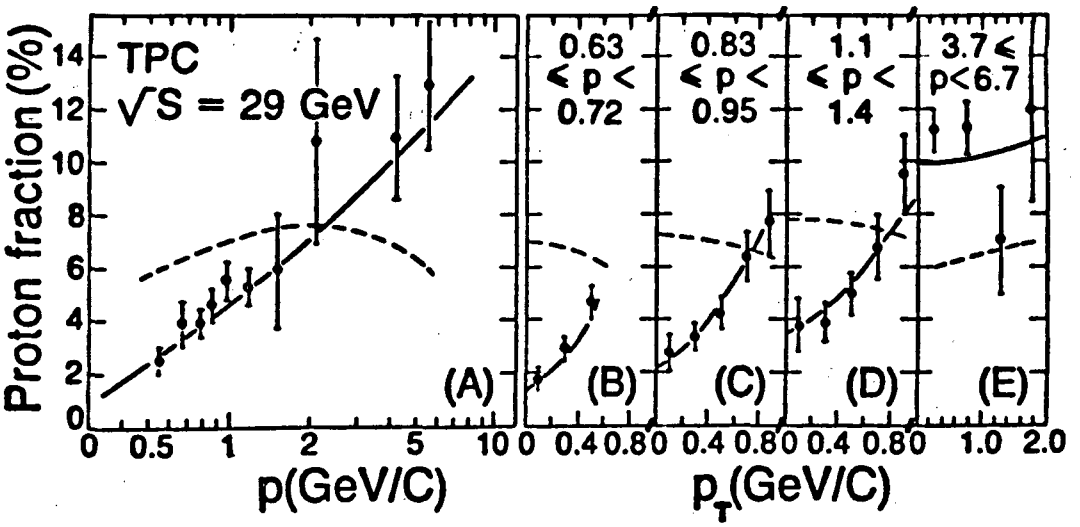

Fig. 19. Fraction of protons among charged particles, measured by the TPC [47], (a) as a function of momentum, (b)-(e) as function of p_T for fixed total momentum. Curves are calculated with the LUND Model for primary hadrons (dashed) and all hadrons (solid).

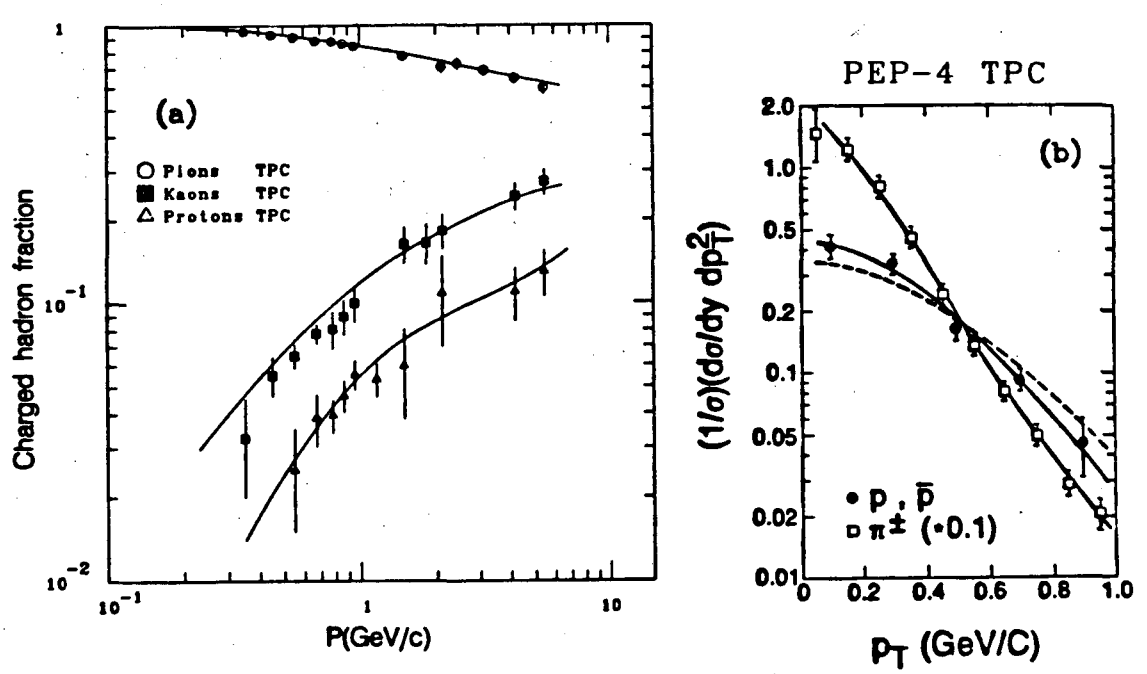

Fig. 20. TPC proton production studies [32,47]. (a) Charged particle fractions as function of momentum, (b) p_T spectra for fixed rapidity ($|y|<1$) for protons and pions.

The proton p_T distribution can also be used to test baryon production mechanisms. If a proton is made out of a diquark and a quark (both of which have the same p_T distribution) the proton mean p_T is expected to be $\cong \sqrt{2}\,(p_T)_q$. If the proton is made out of three independent quarks (all three having the same mean p_T), the mean proton p_T is expected to be $\cong \sqrt{3}\,(p_T)_q$. Included in Fig. 20b are curves obtained with the LUND Monte Carlo for the diquark-quark case (full lines) and with a modified version of the program emulating the three independent quark hypothesis (dashed lines). The diquark-quark model for the proton fits the data very well. The three independent quarks model fits the data also, although it appears to be slightly disfavored.

In conclusion, new data on proton production reported by the TPC [47] points out the effects of resonance decays in the apparent increase of proton production at large p_T. To establish whether this increase is also due to increased proton production in gluon jets, more data are needed and careful studies must be done to disentangle kinematic effects. The study of p_T distributions of protons shows a broader distribution for protons than for pions, this effect can also be explained by resonance decays. Finally with the present statistics, the data cannot distinguish between a baryon production mechanism with three independent quarks and a diquark-quark mechanism, although the latter seems to be favored by the data.

4.4 Two Particle Correlations (TPC).

The study of two particle correlations in e^+e^- annihilation provides information on the hadronization process. The initial state is a massive virtual photon that decays into a $q\bar{q}$ pair (plus possibly a hard gluon) and then in the color field stretched between the two original quarks, other quark pairs are created. At a later time these quarks are transformed into observable hadrons. Correlations between particles that are far apart in rapidity (LRC) provide information on the initial partons and can test flavor compensation. Correlations between particles that are close in rapidity space (SRC) provide information on local conservation of quantum numbers.

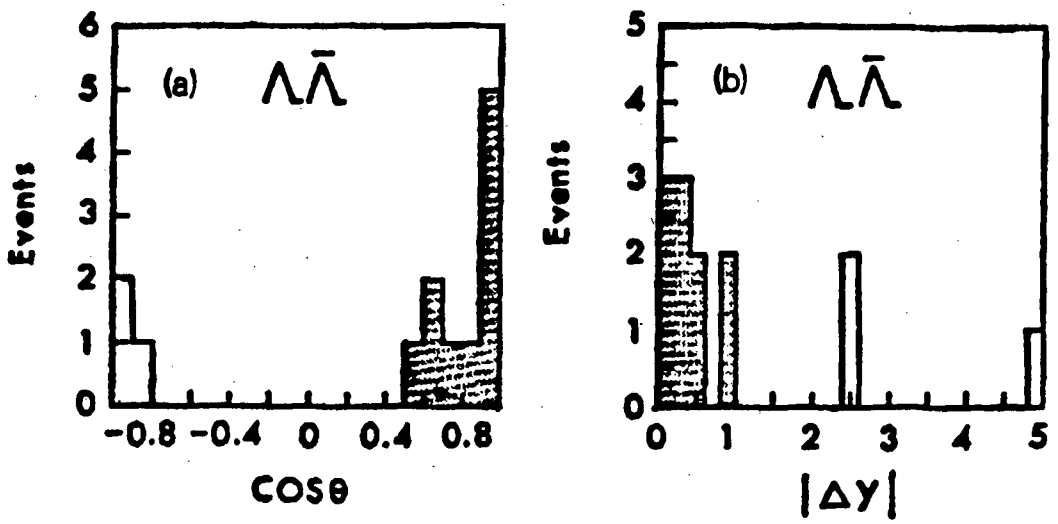

Fig. 21. TPC preliminary results on Λ-$\bar{\Lambda}$ correlations [14]. (a) Opening angle between the Λ and $\bar{\Lambda}$. (b) Distribution of rapidity difference between the Λ and $\bar{\Lambda}$.

The TPC collaboration is reporting Λ-$\bar{\Lambda}$ correlation studies and, using particle identification, presents results on flavor correlations: $\pi\pi$, KK and Kπ [14].

A. Baryon Correlations. Baryons are made of three quarks in a color singlet state. In order to understand the mechanism of baryon production, it is important to know if baryon number is conserved locally, i.e., baryon pairs are produced close in rapidity space or if baryon number is conserved globally, i.e., there is no definite correlation between the baryons produced in a jet. TASSO [51] and JADE [52] have reported data on pp and $\bar{p}$p correlations that show evidence for local baryon compensation.

The TPC collaboration reports new data on Λ-$\bar{\Lambda}$ correlations. In the sample of Λ and $\bar{\Lambda}$ discussed in Sec. 4.2-A there are fourteen events with two entries. They are divided as follows:

Λ-$\bar{\Lambda}$	13 events
Λ-Λ	1 event
$\bar{\Lambda}$-$\bar{\Lambda}$	0 events

Background contribution to the Λ-$\bar{\Lambda}$ sample is estimated

to be 2.2±0.7 events as calculated by the TPC detector simulation that uses the LUND Monte Carlo generator. The distribution of the opening angle between the pair is shown in Fig. 21a. Ten of the thirteen pairs have a small opening angle, which is interpreted to mean that they are produced in the same jet. For each Λ a rapidity is calculated using the sphericity axis as the jet axis. The distribution of $|\Delta y|$, the rapidity difference between the Λ and $\bar{\Lambda}$, is shown in Fig. 21b. On the average, for the ten pairs produced in the same jet, $|\Delta y| = 0.4 \pm 0.3$. This again shows evidence for local baryon compensation.

B. Flavor Correlations. Because of particle identification over a large solid angle, the TPC can study correlations between particles of known flavor. Kaon and pion identification is done using the method discussed in Sec. 4.2-B. For this analysis the requirements on purity are more stringent, and tighter cuts are imposed on the data. The final kaon sample has purity >75% for all rapidity values, whereas the pion sample has purity >90%.

The two particle charge correlations reported by the TASSO collaboration [53] showed evidence for the charged nature of primary partons. A similar technique is used by the TPC collaboration to study $\pi\pi$, KK and $K\pi$ correlations. For each particle in a jet, a rapidity is calculated with respect to the sphericity axis. Then a test particle "a" at a given rapidity y' is chosen and for all other particles of type "b" at rapidity y, a charge density is calculated

$$D(ab)=(N_b(\text{opp. Q as "a"}) - N_b(\text{same Q as "a"}))/N_a$$

The values of D(ab) versus y, for a test particle in the rapidity interval $y'=1.5$ to 4, are plotted in Fig. 22 for the three different cases: $\pi\pi$, KK, πK. The distributions are corrected for acceptance, particle misidentification and radiative effects, using our detector simulation in conjunction with the LUND generator [19]. The corrections are a function of rapidity as well as of the angle of the sphericity axis with respect to the beam line. Error bars in the distributions include the systematic uncertainties associated with these corrections.

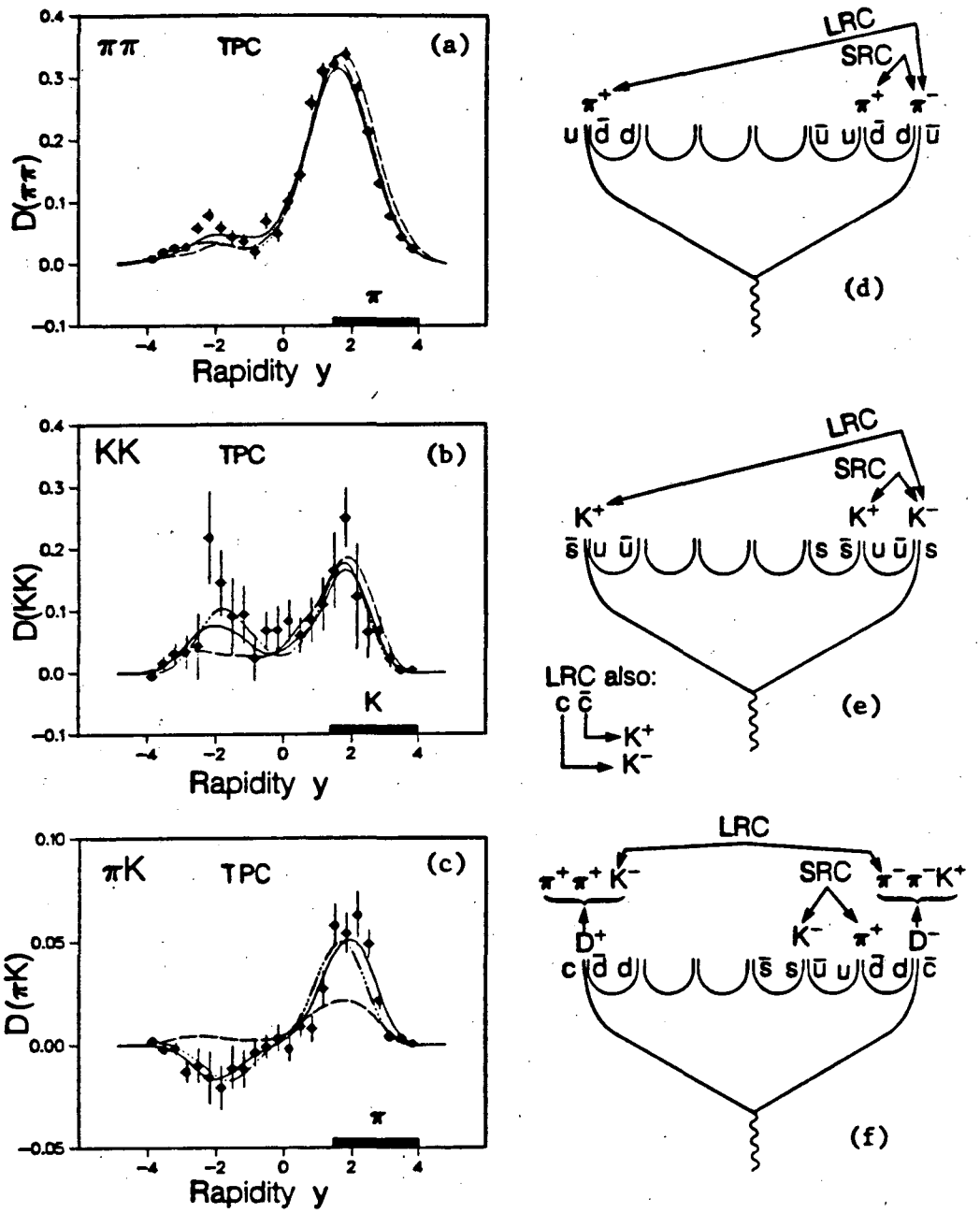

Fig. 22. Flavor tagged charge density, D(ab), versus rapidity y for (a) $\pi^+\pi^-$, (b) K^+K^- and (c) $\pi^\pm K^\mp$. The test particle has y'=1.5-4.0. The solid (dashed) curves show the expected correlation from the LUND Model with (without) c and b quarks. The dot-dashed curves were calculated with the Webber Model [20]. (d)-(f) Show some mechanisms responsible for LRC and SRC.

The $\pi\pi$ correlations in Fig. 22a are similar to the charge correlations reported by TASSO [53] and by Drijard et al. [54] in an ISR experiment. There is a large peak (SRC) at about y=2 due to resonance decays and local charge conservation. A LRC is evident as well; this is evidence for charged primary partons. Integration of the distribution shows that the $\pi^{\pm}$ charge is compensated by another pion (95±2)% of the time.

The KK distribution in Fig. 22b is qualitatively similar to that of Fig. 22a for $\pi\pi$. However, for the KK distribution the relative strengths of the SRC and the LRC are almost equal, whereas for the $\pi\pi$ case the SRC is stronger than the LRC. For the SRC the only known resonance is the ϕ, which, as seen in Table III, is produced at a significant rate and contributes to the effect along with local strangeness compensation. The LRC are due to primary $c\bar{c}$ and $s\bar{s}$ quarks, as indicated in Fig. 22e.

Finally, the $K\pi$ correlation of Fig. 22c illustrates the effect of heavy quark decays. The LRC shows a significant same sign charge correlation. This can be explained with charm production as illustrated in Fig. 22f. The curves drawn in Fig. 22c are the predictions of the "symmetric" LUND model (solid line), of the same model without heavy c and b, quarks (dashed line) and of the Webber [20] model (dot-dashed line). It is clear that most of the observed SRC and LRC are due to heavy quarks. The Webber model and the LUND Model agree with the data for all cases: $\pi\pi$, KK and $K\pi$. It is not possible to distinguish between these two models with the information contained in these graphs.

In conclusion, short and long range flavor correlations have been observed by the TPC collaboration. Short range correlations indicate that quantum numbers are locally conserved. Long range correlations show that the primary quarks carry flavor and that heavy quarks produce sizable effects.

5. SUMMARY

New results from TPC, DELCO, HRS, MAC and MARK II have been presented.

Limits on production of Q = 1/3, 2/3 particles in jets have been improved by about an order of magnitude by the TPC.

A new limit on the mass of the supersymmetric electron has been set by MAC at 35 GeV for zero photino mass.

From the electroweak interference term, new values of the axial weak coupling constant to charm and bottom have been reported by HRS and TPC. The world average of these type of measurements yield (see Table I):

$$a_c = 1.25 \pm 0.34 \qquad a_b = -1.03 \pm 0.24$$

where the Standard Model predicts $a_c = +1$ and $a_b = -1$.

New results on heavy quark fragmentation have been reported by DELCO and TPC. The Peterson et al. [25] form of the fragmentation function fits the data. The ratio of the ϵ parameters obtained from an average of the data is:

$$\epsilon_b/\epsilon_c = 0.07 \pm 0.04$$

in agreement with what is expected from the ratio of the squared masses for charm and bottom ($\cong 0.10$).

New data on jet composition and particle spectra have been reported by HRS, TPC, MARK II, and DELCO. Production of Ξ has been observed which, in conjuction with Λ and proton information, can test some of the assumptions in baryon production models. New data on yields and spectra of K^*, ρ, and ϕ add information relevant to the understanding of the s/u, V/P, and Φ/K^* production ratios.

TPC has made some detailed studies of proton production and emphasized the effect of resonance decays in the apparent increase of the proton fraction with momentum and transverse momentum. The proton p_T distribution is measured to have a Gaussian shape with $\sigma = 0.55 \pm 0.04$ GeV/c.

New results have been presented on two particle correlations, that are expected to provide deeper understanding of the fragmentation process. Local baryon compensation has been observed by the TPC in

Λ-$\bar{\Lambda}$ production. Finally, flavor correlations have been studied by the TPC in e^+e^- annihilation. Both short range and long range flavor compensation are observed in the $\pi\pi$, KK, and Kπ charge-weighted rapidity correlations.

This work was supported by the Department of Energy under contract No. DE-AC03-76SF00098.

REFERENCES

1. H. Aihara et al. (TPC), Phys. Rev. Lett. 52,168 (1984).
2. H. Aihara et al. (TPC), Search for Q=2/3, 1/3 Particles Produced in e^+e^- Annihilation, Lawrence Berkeley Laboratory Report LBL-17551 (March 1984), to be published.
3. J. Burger, Proc. Int Symposium on Lepton and Photon Interactions at High Energies, edited by W. Pfeil (Univ. of Bonn, 1981), p. 115, includes JADE results. J.M. Weiss et al. (MARK II), Phys. Lett. 101B, 439 (1981). M.C. Ross et al. (PEP-14), Phys. Lett. 118B, 199 (1982).
4. M. Piccolo (MAC), Proc. Summer Institute on Particle Physics, Ed. by P. McDonough, SLAC (1983) p. 673. See also, S. Yamada, Proc. Int. Symposium on Lepton and Photon Interactions at High Energies, ed. by D. Cassell and D. Kreinick, Cornell University (1983), p. 525.
5. P. Fayet, Phys. Lett. 117B,460 (1982). J. Ellis and J.S. Hagelin, Phys. Lett. 122B, 303 (1983). T. Kobayashi and M. Kuroda, Report TPR-83-22 (1983), to be published. J.D. Ware and M.E. Machacek, Northeastern Univ. Report NUB-2626 (1984), to be published.
6. E. Ma and J. Okada, Phys. Rev. Lett. 41,287(1978); K.J.F. Gaemers, R. Gastmans et al., Phys. Rev. D19, 1605 (1979).
7. G. Arnison et al. (UA1), Phys. Lett. 126, 398 (1983); B. Sadoulet et al. (UA1), Proc. Int. Symp. On Lepton and Photon Interactions at High Energies, ed. by D. Cassel and D. Kreinick, Cornell University (1983), p. 27.
8. P. Bagnaia et al.(UA2), Phys. Lett. 129B,130 (1983).

9. G. Feldman et al., Phys. Rev. Lett. 38,1313(1977).
10. J.M. Yelton et al. (MARK II), Phys. Rev. Lett. 49 430 (1982). P. Avery et al. (CLEO), Phys. Rev. Lett. 51, 1139 (1983).
11. M. Althoff et al. (TASSO), Phys. Lett. 126B, 493 (1983); also Ref. 13 for asymmetry measurements. S. Ahlen et al. (HRS), Phys. Rev. Lett. 51, 1147 (1983) and private communication.
12. W. Bartel et al. (JADE), presented to the Cornell Conference, see Ref. 13.
13. B. Naroska, Proc. Int. Symp. on Lepton and Photon Interactions at High Energies, ed. by D. Cassel and D. Kreinick, Cornell Univ. (1983), p. 97.
14. H. Aihara et al. (TPC), preliminary results.
15. M.E. Nelson et al.(MARK II), Phys. Rev. Lett. 50, 1542(1983); M.E. Nelson, LBL-16724 (1983), see also Ref. 13. E. Fernandez et al. (MAC), Phys. Rev. Lett. 50, 2054 (1983), and H.S. Kaye, Stanford Linear Accelerator Center Report SLAC-262 (1983), see also Ref. 13 for weak couplings.
16. B. Adeva et al. (MARK J), Phys. Rev. Lett. 51, 443 (1983), see also Ref. 13. M. Althoff et al. (TASSO), DESY 83-121 (1983), to be published. W. Bartel et al. (JADE), unpublished, see Ref. 13 for weak couplings.
17. H. Aihara et al. (TPC), "Prompt Electron Production in e^+e^- Annihilation at 29 GeV," LBL-17545 (March 1984), to be published.
18. P. Hoyer et al. , Nucl. Phys. B161, 349 (1979); A. Ali et al., Phys. Lett. 93B, 155 (1980).
19. B. Andersson, G. Gustafson, G. Ingelsman and T. Sjostrand, Physics Reports 97, 31 (1983); also T. Sjostrand, Comp. Phys. Com. 27, 243 (1982), and 28, 229 (1983). Unless explicitly stated, we use the "Symmetric" LUND Model (JETSET 5.2). When referring to "Standard" LUND we mean JETSET 4.3.
20. B.R. Webber, CERN preprint TH-3713 (1983); G. Marchesini and B.R. Webber, CERN preprint TH-3525 (1983).
21. R.D. Field, S. Wolfram, Nucl. Phys. B213,65(1983).
22. T.D. Gottschalk, Nucl. Phys. B214, 201 (1983); also Caltech preprints CALT-68-1052, 1059 (1983).
23. J. Dorfan, Proc. of the 1983 Int. Symp. on Lepton and Photon Interactions, ed. by D. Cassel and D. Kreinick, Cornell Univ. (1983), p. 686.
24. M. Suzuki, Phys. Lett. 71B, 139 (1977). J.D. Bjorken, Phys. Rev. D17, (1978).

25. C. Peterson et al., Phys. Rev. D27, 105 (1983).
26. G. Goldhaber et al. (MARK II), Phys. Lett. 69B, 503 (1977).
27. D.E. Koop et al. (DELCO), Phys. Rev. Lett. 52, 970 (1984).
28. J.M. Weiss (HRS), Proc. Summer Inst. on Particle Physics, Ed. by P. McDonough, SLAC (1983), p. 643.
29. B. Adewa et al. (MARK J), Phys. Rev. Lett. 51, 443 (1983). M. Althoff et al. (TASSO), DESY 83-121 (1983).
30. M. Althoff et al. (TASSO), preliminary results, quoted by J. Dorfan, Ref. 23.
31. M. Althoff et al. (TASSO), Z. Physik C17, 5 (1983).
32. H. Aihara et al. (TPC), Phys. Rev. Lett. 52, 577 (1983).
33. D. Bender et al. (HRS), "Study of Quark Fragmentation at 29 GeV: Global Jet Parameters and Single Particle Distributions," ANL-HEP-PR-84-09 (1984), to be published.
34. R. Brandelik et al. (TASSO), Phys. Lett. 114B, 65 (1982).
35. H. Aihara et al. (TPC), Nucl. Inst. and Meth. 217, 259 (1983).
36. R. Brandelik et al. (TASSO), Phys. Lett. 108B,71 (1982).
37. H.J. Behrend et al. (CELLO), Z. Physik C20, 207 (1983).
38. M. Althoff et al. (TASSO), Phys. Lett. 130, 340 (1983).
39. H.M. Schellman et al.(MARK II), preliminary result.
40. H. Aihara et al. (TPC), "Φ Meson Production in e^+e^- annihilation at 29 GeV," LBL-17616 (March 1984), to be published.
41. DELCO Collaboration, preliminary result.
42. R. Brandelik et al. (TASSO), Phys. Lett. 117B, 135 (1982).
43. As reported in S.L. Wu, DESY 83-007 (1983) and Proc. Summer Inst. on Particle Physics, Ed. by A. Mosher, SLAC (1982), p. 555.
44. W. Bartel et al.(JADE), Z. Physik C20,187 (1983).
45. M. Althoff et al. (TASSO), Phys. Lett. 136B, 130 (1984).
46. W. Bartel et al. (JADE), Phys. Lett. 130B, 454 (1983).
47. H. Aihara et al. (TPC), "Characteristics of Proton Production in Jets From e^+e^- Annihilation at 29 GeV," LBL-17705 (April 1984), to be published.

48. J.J. Aubert et al. (EMC), Phys. Lett. 135B,225 (1984).
49. H. Albrecht et al., Phys. Lett. 102B,291(1981); also CLEO Collaboration, as reported by J. Dorfan, Ref. 23.
50. G. Schierholz, M. Teper, Z. Physik C13, 53 (1982).
51. M.Althoff et al. (TASSO), Z. Physik C17, 5 (1983); M.Althoff et al., Report DESY 84-4 (to be published).
52. W. Bartel et al.(JADE), Phys. Lett. 104B,325 (1981).
53. R. Brandelik et al. (TASSO), Phys. Lett. 100B, 357 (1981).
54. D. Drijard et al. (ACCDHW), Nucl. Phys. 166B, 233 (1980).

This report was done with support from the Department of Energy. Any conclusions or opinions expressed in this report represent solely those of the author(s) and not necessarily those of The Regents of the University of California, the Lawrence Berkeley Laboratory or the Department of Energy.

Reference to a company or product name does not imply approval or recommendation of the product by the University of California or the U.S. Department of Energy to the exclusion of others that may be suitable.

TECHNICAL INFORMATION DEPARTMENT
LAWRENCE BERKELEY LABORATORY
UNIVERSITY OF CALIFORNIA
BERKELEY, CALIFORNIA 94720